

ARTICLE

# ICOS signaling limits regulatory T cell accumulation and function in visceral adipose tissue

Kristen L. Mittelsteadt<sup>1,2</sup>, Erika T. Hayes<sup>1,2</sup>, and Daniel J. Campbell<sup>1,2,3</sup>

**A unique population of Foxp3<sup>+</sup> regulatory T cells (T<sub>RS</sub>) resides in visceral adipose tissue (VAT) that regulates adipose inflammation and helps preserve insulin sensitivity. Inducible T cell co-stimulator (ICOS) is highly expressed on effector (e)T<sub>RS</sub> that migrate to nonlymphoid tissues, and contributes to their maintenance and function in models of autoimmunity. In this study, we report an unexpected cell-intrinsic role for ICOS expression and downstream phosphoinositide 3-kinase (PI3K) signaling in limiting the abundance, VAT-associated phenotype, and function of T<sub>RS</sub> specifically in VAT. *Icos*<sup>-/-</sup> mice and mice expressing a knock-in form of ICOS that cannot activate PI3K had increased VAT-T<sub>R</sub> abundance and elevated expression of canonical VAT-T<sub>R</sub> markers. Loss of ICOS signaling facilitated enhanced accumulation of T<sub>RS</sub> to VAT associated with elevated CCR3 expression, and resulted in reduced adipose inflammation and heightened insulin sensitivity in the context of a high-fat diet. Thus, we have uncovered a new and surprising molecular pathway that regulates VAT-T<sub>R</sub> accumulation and function.**

## Introduction

CD4<sup>+</sup>Foxp3<sup>+</sup> regulatory T cells (T<sub>RS</sub>) are critical for maintaining immune tolerance and for the resolution of ongoing inflammation after infection (Dominguez-Villar and Hafler, 2018; Noval Rivas and Chatila, 2016; Smigiel et al., 2014a). Specialized subsets of tissue-specific T<sub>RS</sub> also function in tissue repair and homeostasis. For example, Areg<sup>+</sup> T<sub>RS</sub> expand in skeletal muscle and the lungs in response to injury and are required for proper tissue repair (Arpaia et al., 2015; Burzyn et al., 2013), whereas T<sub>RS</sub> within hair follicles and skin are essential for hair generation and inhibiting fibrosis (Ali et al., 2017; Kalekar et al., 2019). T<sub>RS</sub> are also found in the visceral adipose tissue (VAT) of both mice and humans, where they regulate adipose inflammation and preserve metabolic homeostasis (Deiuliis et al., 2011; Eller et al., 2011; Feuerer et al., 2009; Ilan et al., 2010). As such, T<sub>R</sub> ablation in diphtheria toxin-treated Foxp3DTR mice results in increased inflammatory mediators in VAT and reduced insulin sensitivity, whereas augmentation of T<sub>RS</sub> by administration of IL-2 immune complexes or IL-33 results in improved metabolic readouts in mice on a high-fat diet (HFD; Feuerer et al., 2009; Han et al., 2015; Vasanthakumar et al., 2015).

Given that T<sub>RS</sub> modulate diverse responses in different anatomical and inflammatory settings, it is not surprising that they exhibit considerable phenotypic and functional heterogeneity. Expression of CD62L and CD44 broadly divides T<sub>RS</sub> into distinct subsets that are enriched in lymphoid and nonlymphoid tissues

(Campbell, 2015; Smigiel et al., 2014b). We term these populations central T<sub>RS</sub> (cT<sub>RS</sub>) and effector T<sub>RS</sub> (eT<sub>RS</sub>), respectively. Differential activation of phosphoinositide 3-kinase (PI3K), unique epigenetic landscapes, and distinct transcriptional programs underlie the diversification of T<sub>RS</sub>, and selective expression of chemokine receptors and cell adhesion molecules give subsets of T<sub>RS</sub> access to specific tissues (Delacher et al., 2017; DiSpirito et al., 2018; Luo et al., 2016). The proper distribution of T<sub>RS</sub> across tissues is crucial for maintaining immune tolerance and tissue homeostasis (Sather et al., 2007; Yamaguchi et al., 2011). Hence, understanding the signals that control the development, maintenance, and function of tissue-specific T<sub>RS</sub> is vital to fully harnessing their therapeutic potential.

T<sub>R</sub> occupancy in different tissues is met with unique homeostatic maintenance requirements. Generally, IL-2 signaling maintains cT<sub>RS</sub> within T cell zones of secondary lymphoid tissues by driving pro-survival signals, whereas maintenance of eT<sub>RS</sub> in nonlymphoid tissues can be IL-2 independent, and instead relies on TCR and costimulatory molecule engagement (Levine et al., 2014; Smigiel et al., 2014b; Tang et al., 2003). Inducible T cell co-stimulator (ICOS) is expressed on highly suppressive T<sub>RS</sub> and can control T<sub>R</sub> abundance by inhibiting apoptosis and stimulating proliferation (Burmeister et al., 2008; Redpath et al., 2013). IL-10 is essential for control of local immune responses and is primarily expressed by Blimp-1<sup>+</sup>ICOS<sup>+</sup>

<sup>1</sup>Center for Fundamental Immunology, Benaroya Research Institute, Seattle, WA; <sup>2</sup>Molecular and Cellular Biology Program, University of Washington, Seattle, WA; <sup>3</sup>Department of Immunology, University of Washington, Seattle, WA.

Correspondence to Daniel J. Campbell: [dcampbell@benaroyaresearch.org](mailto:dcampbell@benaroyaresearch.org).

© 2021 Mittelsteadt et al. This article is distributed under the terms of an Attribution-Noncommercial-Share Alike-No Mirror Sites license for the first six months after the publication date (see <http://www.rupress.org/terms/>). After six months it is available under a Creative Commons License (Attribution-Noncommercial-Share Alike 4.0 International license, as described at <https://creativecommons.org/licenses/by-nc-sa/4.0/>).

eT<sub>RS</sub> (Cretney et al., 2011). ICOS costimulation in vitro superinduces IL-10 expression (Arimura et al., 2002; Hutloff et al., 1999), and this depends on its ability to activate PI3K (Feito et al., 2003; Okamoto et al., 2003). Although mice deficient in ICOS or ICOS ligand (ICOSL) do not develop spontaneous inflammatory or autoimmune disease, genetic or antibody (Ab)-mediated blockade of ICOS signaling promotes inflammation in mouse models of autoimmunity and infection as a result of reduced T<sub>R</sub> abundance and/or IL-10 production (Busse et al., 2012; Dong et al., 2001; Herman et al., 2004; Kohyama et al., 2004; Kornete et al., 2012; Landuyt et al., 2019; Miyamoto et al., 2005; Redpath et al., 2013).

ICOS potentially activates PI3K and downstream AKT (also known as protein kinase B) via a unique YMFM motif in its cytoplasmic tail (Arimura et al., 2002; Fos et al., 2008). AKT can act on several different substrates, including the transcription factor Foxo1, to modulate transcription of genes involved in proliferation, survival, metabolic reprogramming, and migration/tissue tropism (So and Fruman, 2012). Indeed, inactivation of Foxo1 by AKT is essential for the differentiation of eT<sub>RS</sub> and their migration to nonlymphoid tissues (Luo et al., 2016). The mammalian target of rapamycin (mTOR) pathway is also activated by PI3K signaling and regulates T<sub>R</sub> metabolism and differentiation. Thus, engagement of ICOS may facilitate the development and/or maintenance of eT<sub>RS</sub> via multiple PI3K-dependent signaling pathways.

Accumulation of T<sub>RS</sub> in VAT is dependent on several signals. VAT-T<sub>RS</sub> consist of clonally expanded populations, suggesting that recognition of one or more adipose tissue antigens promotes their tissue residence (Feuerer et al., 2009; Kolodin et al., 2015). Additionally, mice lacking expression of IL-33 or its receptor ST2 are deficient in VAT-T<sub>RS</sub>, whereas injection of exogenous IL-33 results in increased VAT-T<sub>R</sub> abundance with little impact on lymphoid T<sub>RS</sub> (Han et al., 2015; Vasanthakumar et al., 2015). Recent work also identified a cell-intrinsic role for CCR2 in the ability of donor T<sub>R</sub> to repopulate VAT (Vasanthakumar et al., 2020). Finally, T<sub>R</sub> expression of peroxisome proliferator-activated receptor  $\gamma$ , the master regulator of adipocyte differentiation, supports VAT-T<sub>R</sub> phenotype and accumulation and drives expression of factors important for lipid metabolism (Cipolletta et al., 2012; Cipolletta et al., 2015). However, despite having an eT<sub>R</sub> phenotype, the role of costimulatory molecule signaling in VAT-T<sub>RS</sub> is poorly understood.

In this study, we demonstrate an unexpected role for cell-intrinsic ICOS-dependent PI3K signaling in restricting VAT-T<sub>R</sub> accumulation and function. Moreover, we implicate the CCL11/24-CCR3 axis as an additional factor capable of driving recruitment of T<sub>RS</sub> to VAT, which is enhanced in the absence of ICOS signaling. These surprising findings challenge the current model regarding signals that support diverse T<sub>R</sub> subsets and highlight the cell- and tissue-specific effects of ICOS expression and signaling on T<sub>R</sub> development, accumulation, and function.

## Results

### Mice lacking ICOS signaling have reduced T<sub>RS</sub> in lymphoid tissues and altered expression of PI3K targets

To determine how ICOS signaling impacts T<sub>R</sub> abundance in different tissues, we crossed *Foxp3mRFP* mice (Wan and Flavell, 2005) to *Icos*<sup>-/-</sup> (KO) mice and to *IcosY181F* (YF) mice, which carry a tyrosine-to-phenylalanine knock-in mutation in the YMFM motif in the cytoplasmic tail of ICOS, thereby specifically abolishing ICOS-mediated PI3K activation (Gigoux et al., 2009). In line with published data, we found a ~30% reduction in the frequency and number of T<sub>RS</sub> in the spleens of KO compared with WT *Foxp3mRFP* mice (Fig. 1 A; Burmeister et al., 2008; Landuyt et al., 2019). This was even more pronounced in older animals, as T<sub>RS</sub> accumulate with age (Fig. 1 B; Nishioka et al., 2006). Despite normal ICOS expression on the cell surface (Fig. S1 A) and intact MAPK signaling (Gigoux et al., 2009), we saw a similar reduction in splenic T<sub>R</sub> abundance in YF mice, indicating that activation of PI3K signaling is the critical pathway by which ICOS regulates T<sub>R</sub> abundance (Fig. 1, A and B). ICOS is expressed on cT<sub>RS</sub>, but its expression is further up-regulated on eT<sub>RS</sub> (Fig. S1 B). The loss of T<sub>RS</sub> we observed in YF and KO spleens was associated with a disproportionate reduction in the frequency and number of eT<sub>RS</sub>, whereas cT<sub>R</sub> abundance was unchanged, consistent with results using Ab blockade of ICOS signaling (Fig. 1 C; Smigiel et al., 2014b). Loss of T<sub>RS</sub> was also observed in the peripheral LNs (pLNs) of YF and KO mice, indicating that ICOS signaling is important for eT<sub>R</sub> maintenance in multiple secondary lymphoid organs (Fig. S1 C). Both YF and KO T<sub>RS</sub> in the spleen had elevated expression of the lymphoid homing molecules CD62L and CCR7, which are down-regulated upon PI3K activation via phosphorylation and sequestration of Foxo1 (Fig. 1 D; Kerdiles et al., 2009). This reflects both an increased frequency of splenic cT<sub>RS</sub> as well as increased CD62L and CCR7 expression by gated CD44hi T<sub>RS</sub> in YF and KO mice. When examined directly ex vivo, YF and KO splenic T<sub>RS</sub> also exhibited reduced phosphorylation of the mTORC1 target, ribosomal protein S6, consistent with diminished activation of PI3K (Fig. 1 E). Thus, the absence of ICOS-mediated PI3K activation drives the altered lymphoid T<sub>R</sub> frequency and phenotype in YF and KO mice.

### T<sub>RS</sub> are enriched in VAT in the absence of ICOS signaling

As eT<sub>RS</sub> are highly enriched in nonlymphoid sites (Lee et al., 2007; Smigiel et al., 2014b), we next assessed whether maintenance of T<sub>RS</sub> in peripheral tissues was diminished in YF and KO mice. Using intravascular labeling to identify tissue-localized T<sub>RS</sub> (Anderson et al., 2014), we observed a reduction in the frequency and number of T<sub>RS</sub> in the skin and a decrease in the absolute number of T<sub>RS</sub> in the lungs of YF and KO mice (Fig. 2, A and B). However, T<sub>R</sub> frequency and total number were actually elevated in the VAT of both ICOS mutant strains (Fig. 2 C). This was specific to VAT, as frequency and total number of T<sub>RS</sub> in subcutaneous adipose tissue (SQAT) remained similar between genotypes (Fig. 2 D). Male and female YF and KO mice demonstrated increased VAT-T<sub>R</sub> abundance compared with WT mice of the same sex; however, the frequency and number of VAT-T<sub>RS</sub> in females was significantly less than that observed in males (Fig. 2,

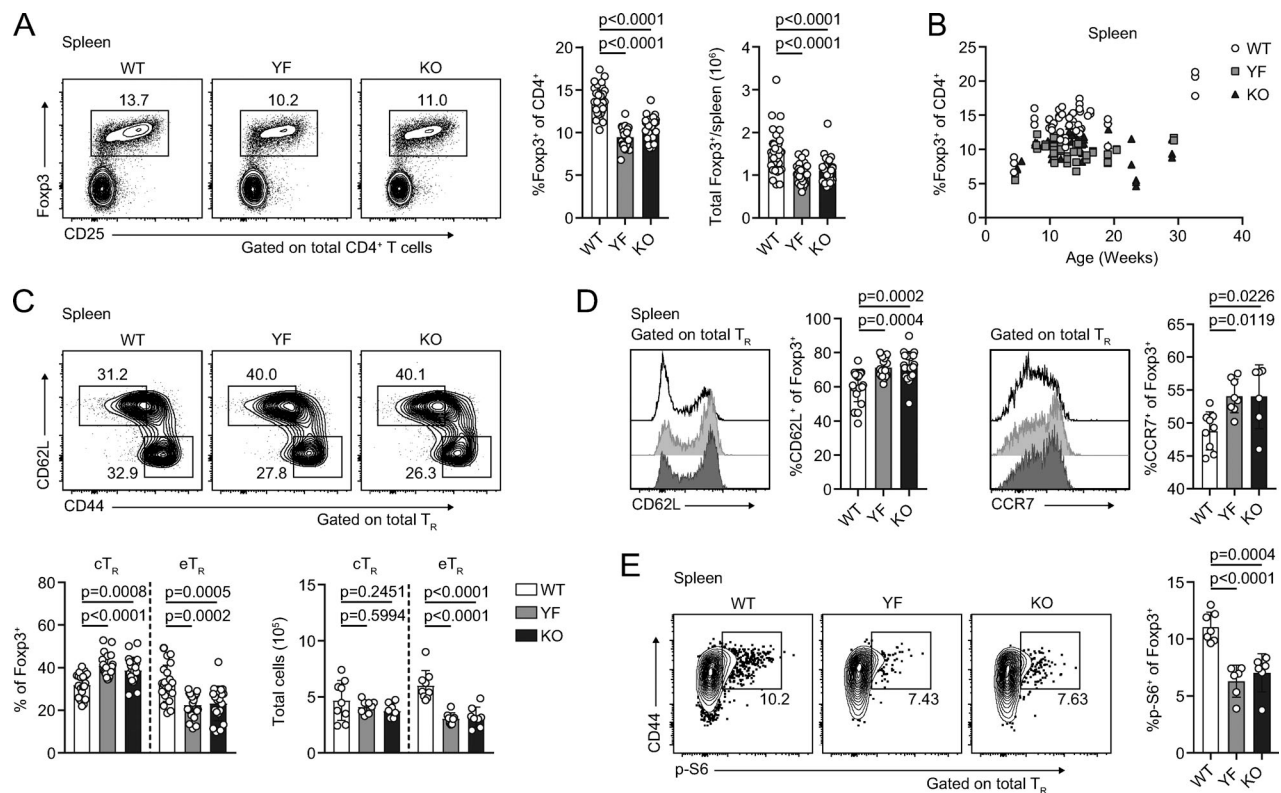


**Figure 1. Absence of ICOS signaling results in loss of lymphoid T<sub>R</sub>s and altered expression of PI3K targets.** (A) Representative flow cytometry plots and quantification of splenic T<sub>R</sub>s (*n* = 3–6 per group from nine independent experiments). (B) Splenic T<sub>R</sub> frequencies at indicated ages (*n* = 3–5 per group from 16 independent experiments). (C) Representative flow cytometry plots and quantification of splenic cT<sub>R</sub>s (CD44<sup>lo</sup>CD62L<sup>hi</sup>) and eT<sub>R</sub>s (CD44<sup>hi</sup>CD62L<sup>lo</sup>; *n* = 3–5 per group from seven independent experiments). (D) Expression of CD62L and CCR7 in splenic T<sub>R</sub>s (CD62L: *n* = 3–5 per group from five independent experiments; CCR7: *n* = 3–5 per group from two independent experiments). (E) S6 phosphorylation (p-S6) measured directly ex vivo in splenic T<sub>R</sub>s by flow cytometry (*n* = 3 or 4 per group from two independent experiments). Mice were age matched within independent experiments, and pooled data are from experiments using mice aged 8–16 wk, except in B, where age is indicated. Statistical significance was determined using one-way ANOVA with Tukey’s post-test. All graphical data are presented as mean values ± SD.

E and F). Consistent with previous studies, we observed age-dependent accumulation of VAT-T<sub>R</sub>s across all three genotypes in male mice (Feuerer et al., 2009), but despite considerable mouse-to-mouse variability, VAT-T<sub>R</sub>s remained elevated in YF and KO mice across all age groups analyzed (Fig. 2 G).

We used male mice for the remainder of our studies as we found female mice harbor approximately fourfold to fivefold fewer T<sub>R</sub>s/gram VAT than age-matched males, and female mice are protected from the development of diet-induced metabolic syndrome (Ahnstedt et al., 2018; Pettersson et al., 2012; Vasanthakumar et al., 2020). The frequency of VAT-T<sub>R</sub>s expressing KLRG1 and CD69 was significantly elevated in YF and KO mice compared with WT controls (Fig. 3 A). By contrast, in the spleen there was a reduced frequency of YF and KO T<sub>R</sub>-expressed CD69, and very few T<sub>R</sub>s were KLRG1<sup>+</sup> (Fig. S2 A). We assessed VAT-T<sub>R</sub> Foxp3 and CD44 expression and found no difference in the absence of ICOS (Fig. S2 B). We did, however, observe a modest increase in the expression of CTLA-4 and a slight reduction in the frequency of CD25<sup>+</sup> T<sub>R</sub>s in YF and KO VAT (Fig. 3 A). Therefore, T<sub>R</sub>s in the VAT of YF and KO mice are enriched in expression of markers indicative of an eT<sub>R</sub> and VAT-T<sub>R</sub> phenotype (Feuerer et al., 2009; Smigielski et al., 2014b).

In addition to prototypical eT<sub>R</sub> markers, a fraction of VAT-T<sub>R</sub>s express the IL-33 receptor ST2 (Kolodin et al., 2015; Vasanthakumar et al., 2015). Signaling downstream of ST2 is required for the establishment and maintenance of VAT-T<sub>R</sub>s, and expansion of VAT-T<sub>R</sub>s through administration of IL-33 can reduce VAT inflammation and improve metabolic indices in models of diet-induced obesity (Han et al., 2015; Kolodin et al., 2015; Vasanthakumar et al., 2015). In addition to ST2-expressing T<sub>R</sub>s, we found a substantial population of CXCR3<sup>+</sup> T<sub>R</sub>s in the VAT of lean mice, confirming previously reported findings (Fig. 3 B; Li et al., 2018). Although there were no significant differences in the frequency of WT, YF, or KO VAT-T<sub>R</sub>s singly expressing ST2 or CXCR3, we found a unique population of double-expressing ST2<sup>+</sup>CXCR3<sup>+</sup> T<sub>R</sub>s in YF and KO VAT, which resembled canonical VAT-T<sub>R</sub>s in their expression of KLRG1 and CD69 (Fig. 3, B and C). Furthermore, whereas the abundance of splenic T<sub>R</sub>s in WT mice was dramatically reduced following treatment with the mTORC1 inhibitor rapamycin, there was no significant change in the number of T<sub>R</sub>s in the VAT (Fig. S2 C), indicating that ICOS-dependent PI3K activation regulates VAT T<sub>R</sub>s independently of mTORC1 activity.

ICOS signaling can potentiate IL-10 production (Busse et al., 2012; Dong et al., 2001; Herman et al., 2004; Hutloff et al., 1999;

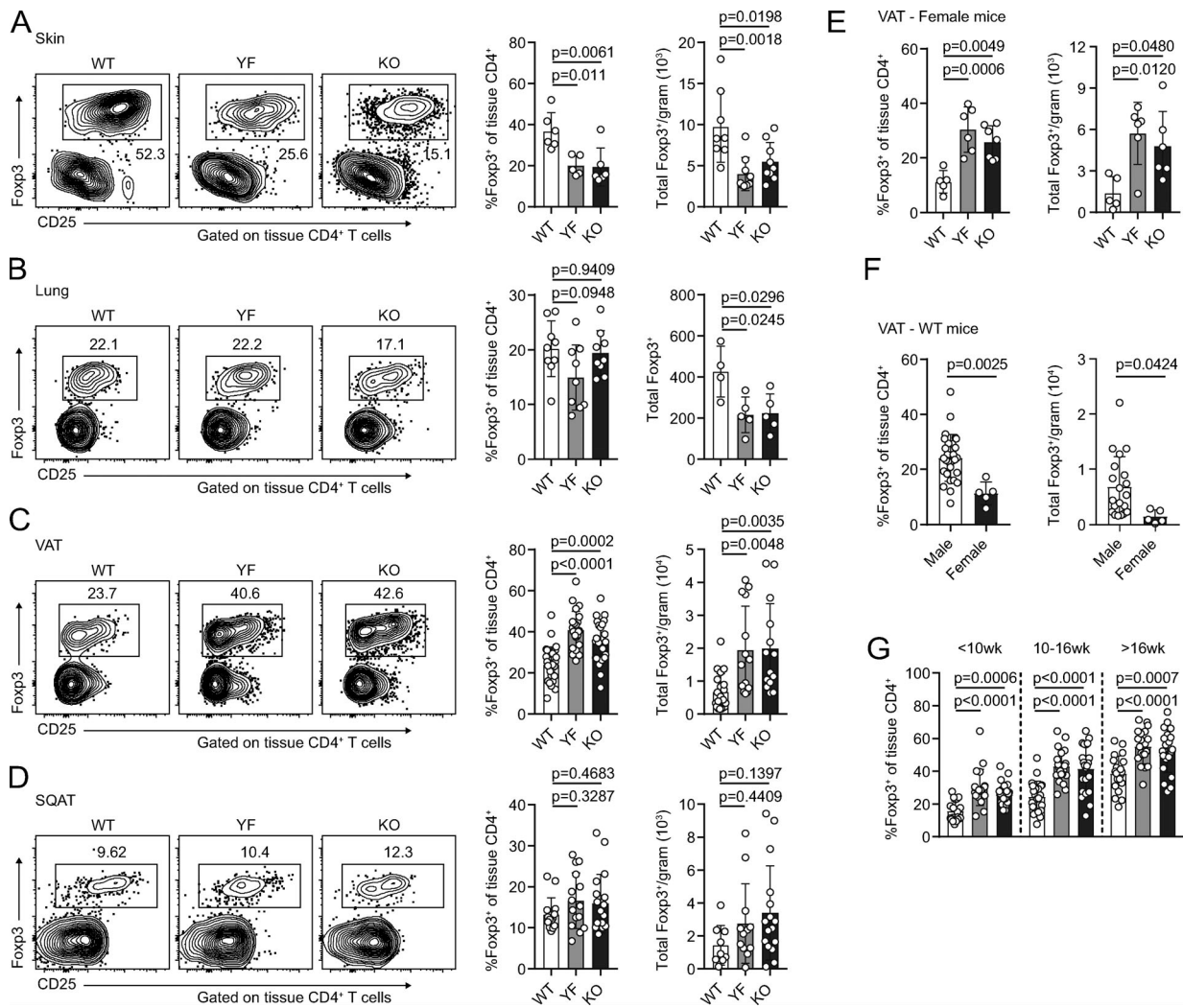


**Figure 2. T<sub>R</sub> frequency and number are increased in VAT in the absence of ICOS signaling. (A–D)** Representative flow cytometry plots and quantification of T<sub>R</sub>S among tissue-localized TCRβ<sup>+</sup>CD4<sup>+</sup> cells in WT, YF, and KO ear skin (A), lung (B), VAT (C), and inguinal SQAT (D) of male mice (skin: n = 3 per group from two independent experiments; lung: n = 3 per group from three independent experiments; VAT: n = 3–6 from eight independent experiments; SQAT: n = 3–5 for five independent experiments). **(E)** Tissue-localized VAT-T<sub>R</sub> frequency and total number in female WT, YF, and KO mice (n = 3 per group for three independent experiments). **(F)** T<sub>R</sub> frequency and total number in VAT of male versus female WT mice (combined data from C and E). **(G)** VAT-T<sub>R</sub> frequencies by noted age bins in male mice as measured by flow cytometry (n = 3–5 mice per group from 18 independent experiments). Mice were age matched within independent experiments, and pooled data are from experiments using mice aged 8–16 wk, except in G, where age is indicated. Statistical significance was determined using one-way ANOVA with Tukey’s post-test or two-tailed Student’s t test where appropriate. All data are presented as mean values ± SD.

Kohyama et al., 2004; Kornete et al., 2012; Landuyt et al., 2019; Miyamoto et al., 2005; Redpath et al., 2013). Surprisingly, compared with VAT-T<sub>R</sub>S from WT mice, a substantially higher frequency of YF and KO VAT-T<sub>R</sub>S were poised to produce IL-10 upon ex vivo stimulation with phorbo-myristate-acetate and ionomycin (PMA/I), with no appreciable differences in IL-10 expression by splenic T<sub>R</sub>S (Fig. 3 D). Thus, absence of ICOS-dependent PI3K signaling supports both the accumulation and suppressive phenotype of T<sub>R</sub>S in VAT.

**Baseline adipose inflammation is reduced in YF and KO mice**

VAT inflammation is modulated through a balance of different immune cells. T<sub>R</sub>S, eosinophils, anti-inflammatory adipose tissue macrophages (ATMs), and type 2 innate lymphoid cells (ILC2s) maintain a type 2 immune environment that supports

metabolic homeostasis in lean animals. Inflammation drives recruitment of neutrophils and cytotoxic T cells, differentiation of inflammatory ATM, and production of pro-inflammatory cytokines like TNFα (Burhans et al., 2019; Molofsky et al., 2013). Although there was no difference in mouse weights between WT, YF, and KO mice across different ages, we did observe a trend toward increased VAT weight in YF mice and a significant increase in KO mice (Fig. 4 A). By histology, we did not observe any overt morphological differences in VAT from WT, YF, and KO mice, including no observable differences in adipocyte size (Fig. S3 A). The increase in VAT weight, however, did correlate with a modest increase in the total number of CD4<sup>+</sup> effector T cells (T<sub>eff</sub>S) per gram of tissue (Fig. 4 B). Despite this increase in VAT-T<sub>eff</sub> number, there was a substantially lower frequency of YF and KO VAT-T<sub>eff</sub>S expressing features of

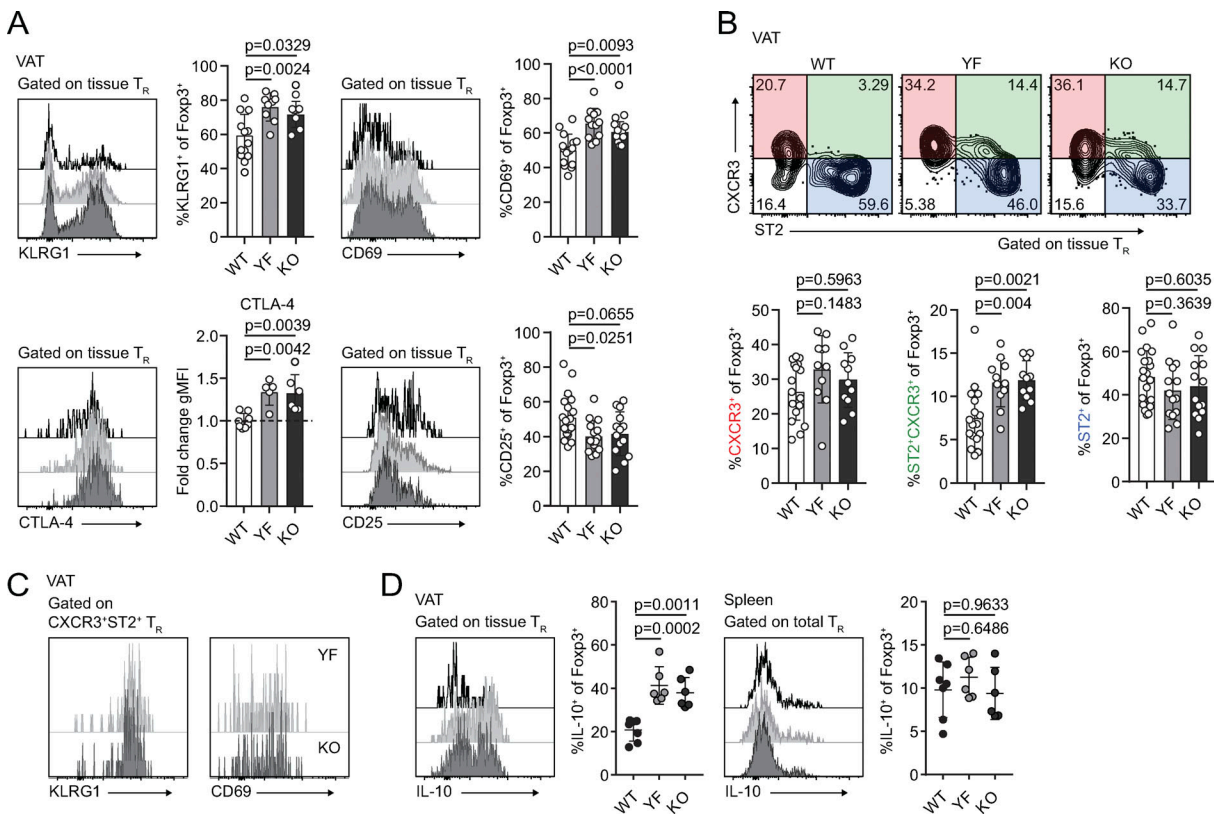


**Figure 3. Loss of ICOS signaling supports an e $T_R$  phenotype in VAT. (A)** Representative flow cytometry plots and quantification of KLRG1, CD69, CTLA-4, and CD25 expression in tissue-localized VAT- $T_R$ s. CTLA-4 gMFI was calculated as fold change compared with average expression in WT  $T_R$ s for each individual experiment. Dashed line marks average value of WT control samples ( $n = 3-6$  per group from three independent experiments or, for CTLA-4, two independent experiments). **(B)** Representative gating of VAT- $T_R$ s on CXCR3 and ST2 expression and quantification of VAT- $T_R$ s positive for CXCR3 (left) or ST2 (right) alone or double-expressers of CXCR3 and ST2 (middle;  $n = 3-5$  per group from five independent experiments). **(C)** Representative histograms showing expression of KLRG1 and CD69 in CXCR3<sup>+</sup>ST2<sup>+</sup> YF and KO VAT- $T_R$ s as measured by flow cytometry. **(D)** Representative flow cytometry plots and quantification of IL-10 expression in  $T_R$ s from VAT and spleen after 4-h PMA/I + monensin stimulation ex vivo ( $n = 3-5$  per group from two independent experiments). Mice were age matched within independent experiments, and pooled data are from experiments using male mice aged 8-16 wk. Statistical significance was determined using one-way ANOVA with Tukey's post-test. All data are presented as mean values  $\pm$  SD.

inflammatory T helper type 1 cells (Th1 cells), including CXCR3, IFN- $\gamma$ , and TNF $\alpha$  (Fig. 4 C). Rather, ST2-expressing  $T_{eff}$ s were enriched in YF and KO VAT (Fig. 4 C). Similar to VAT- $T_R$ s, YF and KO VAT- $T_{eff}$ s were superior at producing IL-10 upon stimulation, suggesting that absence of ICOS signaling in  $T_{eff}$ s supports a self-regulatory function (Fig. 4 C). IL-33 signaling induces production of Th2 cytokines (Schmitz et al., 2005), which maintain ATMs in an anti-inflammatory state. While we didn't find any significant changes in ATM or ILC2 populations (Fig. S3, B and C), we did note an increased frequency of eosinophils in YF and KO VAT (Fig. 4 D), which produce IL-4 to maintain anti-inflammatory ATMs (Molofsky et al., 2013; Wu et al., 2011). Overall, global loss of ICOS expression and signaling impacts  $T_R$ s along with other adipose-resident immune cells to maintain an anti-inflammatory state in VAT.

#### YF and KO mice are protected from HFD-induced insulin resistance

Given the abundance and suppressive phenotype of  $T_R$ s and other anti-inflammatory immune cells in VAT in YF and KO

mice, we asked if they were more resistant to developing HFD-induced adipose inflammation and metabolic changes. Mice placed on an 18-wk HFD steadily gained body mass, with a modest reduction in weight gained by KO mice compared with WT (Fig. 5 A). After 18 wk on HFD, YF and KO mice sustained elevated  $T_R$  frequencies in VAT compared with WT mice, with an increased fraction of cells expressing the canonical VAT- $T_R$  markers ST2 and KLRG1 and a smaller proportion of  $T_R$ s expressing CXCR3 (Fig. 5, B and C). Additionally, YF and KO mice placed on an HFD retained a greater frequency of eosinophils, and  $T_{eff}$ s skewed toward a type 2, ST2-expressing phenotype (Fig. 5, D and E). Fasting blood glucose levels (BGLs) were similar among genotypes after 18 wk, and WT, YF, and KO mice were able to clear glucose to the same extent, as measured by glucose tolerance test (GTT; Fig. 5 F). However, in an insulin tolerance test (ITT), YF and KO mice demonstrated improved insulin sensitivity compared with WT mice (Fig. 5 G). Thus, loss of ICOS supports  $T_R$ s and other anti-inflammatory cells in VAT during an HFD, and this has functional consequences in maintaining metabolic homeostasis.

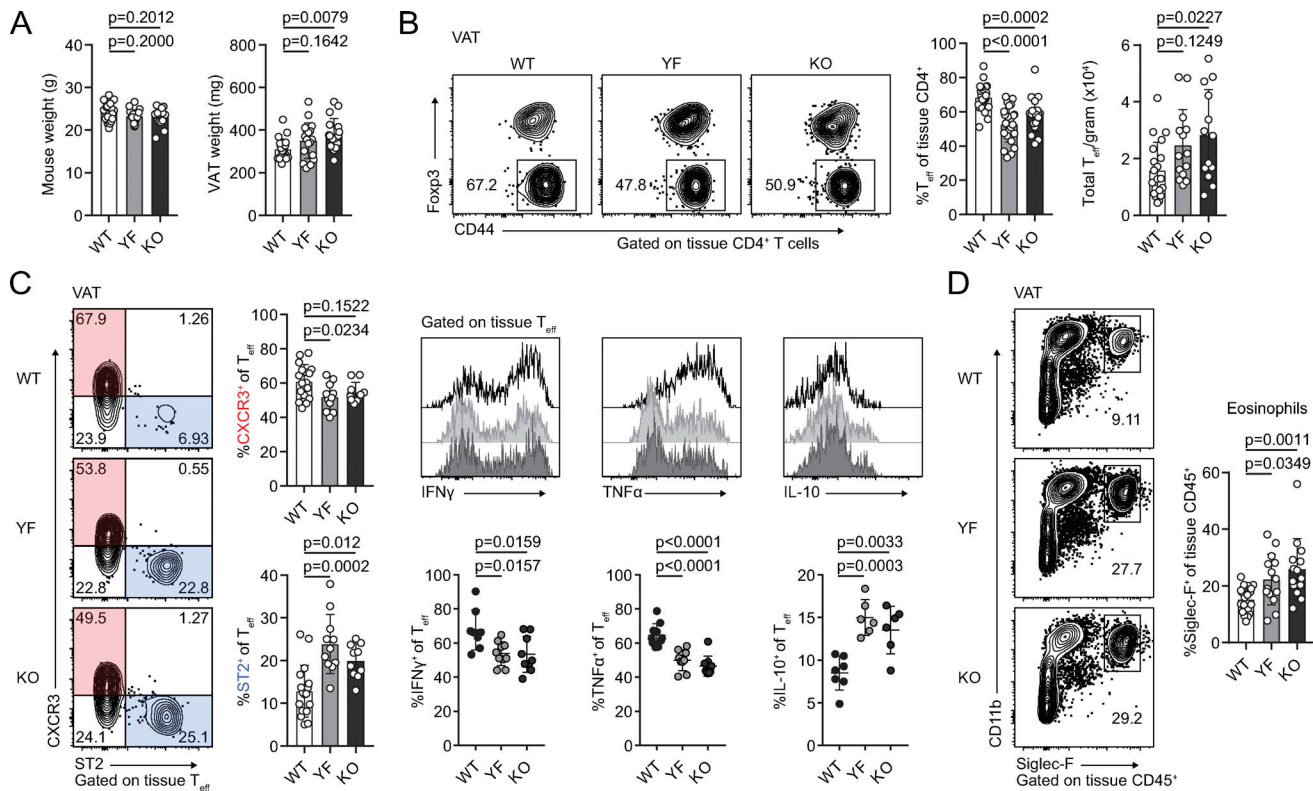


**Figure 4. Reduced expression of inflammatory markers in YF and KO VAT.** (A) Summary of total mouse and VAT weight in male WT, YF, and KO mice ( $n = 3-6$  per group from six independent experiments). (B) Representative flow cytometry plots and quantification of tissue-localized VAT- $T_{reg}$ s in WT, YF, and KO mice ( $n = 3-6$  per group from eight independent experiments). (C) Representative gating of VAT- $T_{reg}$ s on CXCR3 and ST2 expression and quantification of VAT- $T_{reg}$ s positive for CXCR3 or ST2 (left;  $n = 3-5$  per group from five independent experiments). Representative flow cytometry plots (top panels) and quantification (bottom panels) of IFN- $\gamma$ , TNF $\alpha$ , and IL-10 expression in VAT- $T_{reg}$ s after 4-h PMA/I + monensin stimulation ex vivo (right;  $n = 3-5$  per group from two independent experiments). (D) Tissue-localized eosinophil frequencies in VAT ( $n = 2-6$  from six independent experiments). Mice were age matched within independent experiments, and pooled data are from experiments using male mice aged 8-16 wk. Statistical significance was determined using one-way ANOVA with Tukey's post-test. All graphical data are presented as mean values  $\pm$  SD.

### Absence of ICOS supports the accumulation and phenotype of VAT- $T_{reg}$ s in a cell-intrinsic manner

ICOS signaling supports a wide array of cellular processes in the context of adaptive immunity (Panneton et al., 2019). To determine which of the T cell phenotypes we observed in intact YF and KO mice were the result of cell-intrinsic ICOS expression and signaling, we generated mixed bone marrow chimeras using congenically marked  $CD45.1^+$  WT and  $CD45.2^+$  WT, YF, or KO donors (Fig. 6 A). Body and adipose depot weights were similar between groups of chimeric mice (Fig. S4 A). Consistent with the increased abundance of VAT- $T_{reg}$ s that we observed at baseline in intact YF and KO mice, both  $CD45.2^+$  YF and KO  $T_{reg}$ s displayed a competitive advantage compared with  $CD45.1^+$  WT  $T_{reg}$ s in repopulating VAT in our chimeric mice. Whereas WT:WT chimeras reconstituted VAT- $T_{reg}$ s at an  $\sim 1:1$  ratio, YF and KO  $T_{reg}$ s exhibited a significantly higher reconstitution ratio of  $\sim 5.5:1$  (Fig. 6 B). In addition to supporting VAT- $T_{reg}$  abundance, absence of cell-intrinsic ICOS signaling also promoted a canonical VAT- $T_{reg}$  phenotype. Within the same chimeras, a higher frequency of YF and KO VAT- $T_{reg}$ s expressed CD69 and ST2 (Fig. 6 C). Aligned with data from intact mice, more YF and KO VAT- $T_{reg}$ s within chimeras were double-expressers of CXCR3 and ST2 (Fig. 6 C). Functionally, a larger proportion of YF and KO VAT-

$T_{reg}$ s were poised to produce IL-10 after ex vivo stimulation (Fig. 6 C). Mixed bone marrow chimeras retain a population of radioresistant host  $T_{reg}$ s, which proliferate to replenish a portion of the available niche after irradiation (Komatsu and Hori, 2007), and this is particularly evident in many nonlymphoid tissues. Remarkably, in addition to preferentially reconstituting VAT compared with WT donor  $T_{reg}$ s, YF and KO VAT- $T_{reg}$ s were able to outcompete endogenous WT VAT- $T_{reg}$ s as well, nearly replacing the entire  $T_{reg}$  compartment in some chimeras (Fig. 6 D).

Contrary to our findings in VAT, YF and KO  $T_{reg}$ s were at a selective disadvantage in the skin, spleen, and large intestine, with no difference in reconstitution in the lungs (Fig. 6 E and Fig. S4 B).  $T_{reg}$ s found in SQAT are phenotypically distinct from VAT- $T_{reg}$ s and do not appear to accumulate with age (Feuerer et al., 2009; Li et al., 2018). However, unlike in intact mice, we did note that YF and KO donor  $T_{reg}$ s displayed a competitive advantage in repopulating SQAT in chimeric mice at a ratio of  $\sim 3:1$  (Fig. 6 E). This could be due to low-level inflammation following irradiation of the recipient mice that drives reconstitution of the SQAT niche, with  $T_{reg}$ s exhibiting a VAT- $T_{reg}$  phenotype.

Although  $CD8^+$  T cells and ILC2s of either genotype were similarly represented (Fig. S4 C), we did find that YF and KO

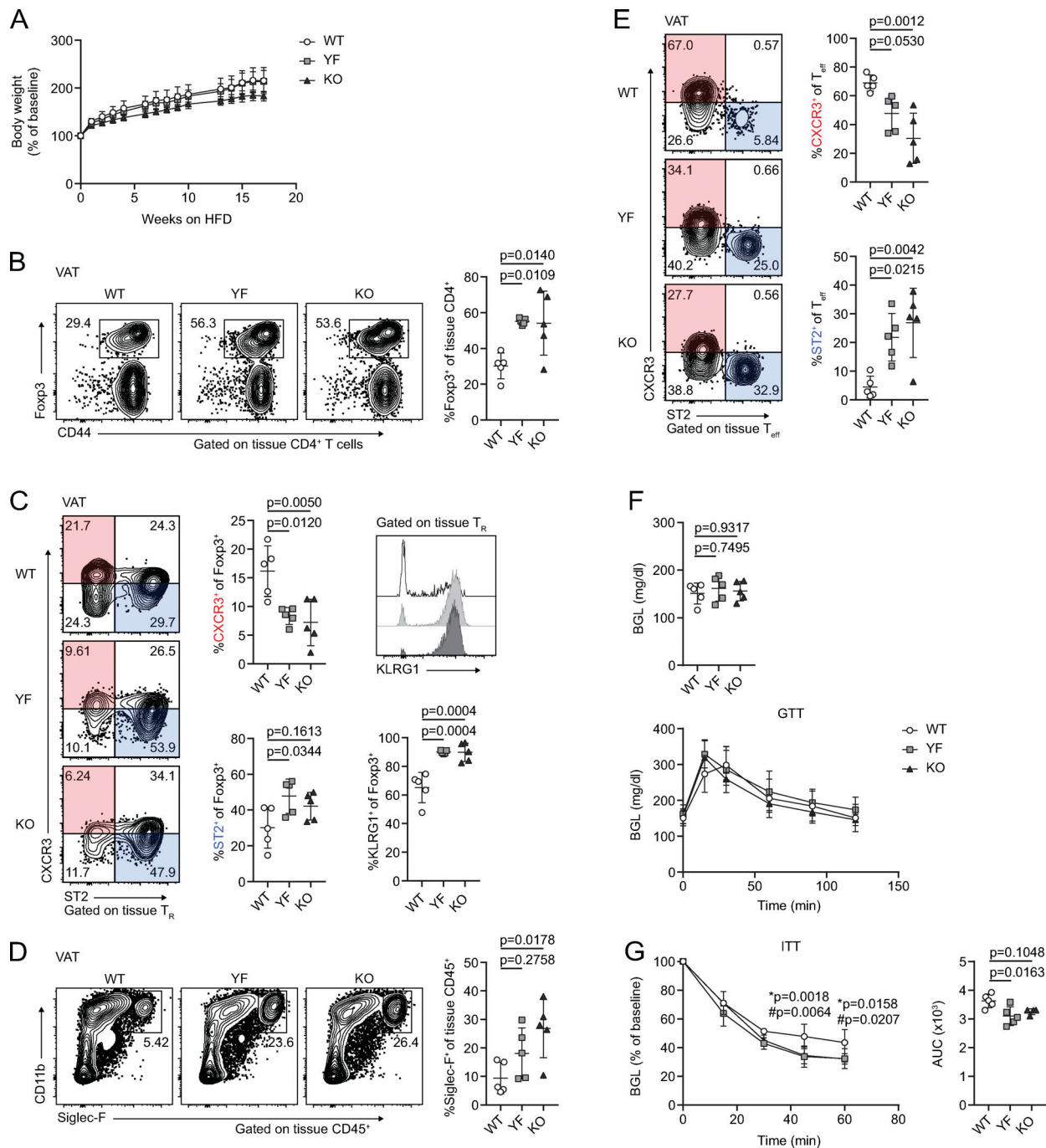


**Figure 5. Mice deficient in ICOS signaling maintain anti-inflammatory immune cell abundance and phenotype in VAT after a long-term HFD, correlating with improved insulin sensitivity.** (A) Percentage of baseline body weight at indicated time points following initiation of an HFD. (B) Tissue-localized VAT-T<sub>R</sub> frequency after 18 wk of an HFD. (C) VAT-T<sub>R</sub> phenotypic data as measured by flow cytometry showing expression of CXCR3, ST2, and KLRG1. (D) Frequency of tissue-localized eosinophils in VAT. (E) Representative gating of VAT-T<sub>eff</sub>s on CXCR3 and ST2 with summarized graphical data. (F) Fasting BGL (top) and GTT (bottom) in HFD-fed mice. (G) ITT in HFD-fed mice. \* indicates significant difference between WT and YF; # indicates significant difference between WT and KO. ITT area under the curve (AUC) was calculated for each individual mouse. All data are representative of two independent experiments with *n* = 4 or 5 per group. For weight (A), GTT (F), and ITT (G), statistical significance was determined using two-way repeated-measures ANOVA with Tukey's post-test for multiple comparisons. For fasted BGL (F), ITT AUC (G), and all flow cytometry summary graphs, statistical significance was determined using one-way ANOVA with Tukey's post-test. All graphs are presented as mean values ± SD.

T<sub>eff</sub>s were modestly, but significantly, enriched in VAT at a ~2:1 ratio compared with WT T<sub>eff</sub>s, with no difference in reconstitution of other tissues (Fig. 6 F). A higher frequency of YF and KO VAT-T<sub>eff</sub>s were ST2<sup>+</sup> within the same chimeras, with a

reduction in CXCR3-expressing T<sub>eff</sub>s (Fig. 6 G). Functionally, YF and KO VAT-T<sub>eff</sub>s were composed of fewer IFN-γ<sup>+</sup> and TNFα<sup>+</sup> and more IL-10<sup>+</sup> cells when stimulated ex vivo (Fig. 6 G), indicating that in addition to driving increased T<sub>R</sub> abundance, the

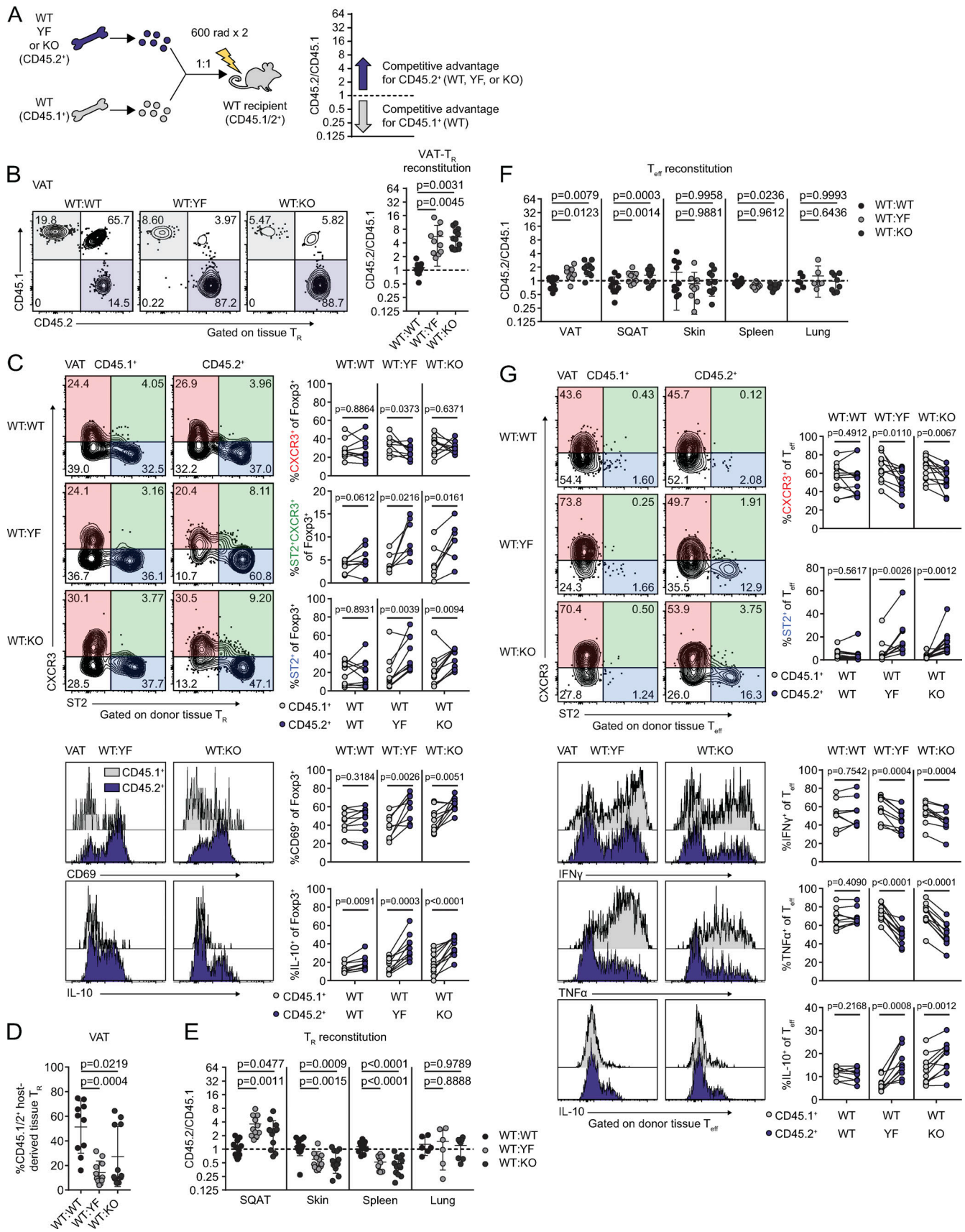


Figure 6. Cell-intrinsic ICOS signaling limits T<sub>R</sub> and T<sub>eff</sub> abundance and phenotype in VAT. (A) Schematic of mixed bone marrow chimera setup (left) and analysis (right). The dashed line in all subsequent graphs indicates a CD45.2/CD45.1 ratio of 1. (B) Representative gating of CD45.1 versus CD45.2 expression in

chimeric mice on tissue-localized T<sub>R</sub>S in VAT and quantification of donor T<sub>R</sub> reconstitution in VAT. **(C)** Representative gating on CXCR3- and ST2-expressing CD45.1<sup>+</sup> and CD45.2<sup>+</sup> donor VAT-T<sub>R</sub>S in chimeric mice (top). Lines connect points indicating CD45.1<sup>+</sup> and CD45.2<sup>+</sup> cells within the same chimeric mouse. Histogram and quantification of CD69 expression in donor VAT-T<sub>R</sub>S. Histogram and graphical summary of donor VAT-T<sub>R</sub> expression of IL-10 after 4-h PMA/I + monensin stimulation ex vivo (bottom). **(D)** Frequency of endogenous CD45.1/2<sup>+</sup> VAT-T<sub>R</sub>S in chimeric mice. **(E)** Reconstitution of donor T<sub>R</sub>S in the indicated tissues. **(F)** Summary of donor T<sub>eff</sub> reconstitution in the indicated tissues. **(G)** CXCR3 and ST2 expression by gated VAT-T<sub>eff</sub> (top). Histograms and summary of donor VAT-T<sub>eff</sub> expression of IFN- $\gamma$ , TNF $\alpha$ , and IL-10 after 4-h PMA/I + monensin stimulation ex vivo (bottom). Data are pooled from three independent experiments with  $n = 3-5$  per group. Statistical significance for cell population reconstitution was determined using one-way ANOVA with Tukey's post-test for each tissue analyzed. Data are presented as mean values  $\pm$  SD. A two-tailed, paired Student's  $t$  test was used to assess statistical significance when comparing expression in donor cells within the same chimeric mouse.

absence of ICOS signaling also promotes a regulatory phenotype in VAT-T<sub>eff</sub>S. Taken together, loss of ICOS signaling supports VAT-T<sub>R</sub> and, to a lesser extent, T<sub>eff</sub> accumulation and phenotype through cell-intrinsic mechanisms.

### ICOS signaling impacts expression of homing receptors in T<sub>R</sub>S that allow access to VAT

The increased abundance of VAT-T<sub>R</sub>S from YF and KO mice could result from the combination of increased proliferation, increased survival, or increased migration to the VAT. The proliferation marker Ki67 was expressed by ~10–20% of VAT-T<sub>R</sub>S, and we found no significant difference in the frequency of Ki67<sup>+</sup> VAT-T<sub>R</sub>S between WT, YF, and KO mice (Fig. 7 A). Similarly, WT, YF, and KO VAT-T<sub>R</sub>S expressed similar levels of the prosurvival protein Bcl2 (Fig. 7 B). Despite the lack of differences in Ki67 or Bcl-2 expression, we cannot rule out that changes in cellular turnover contribute to the differences we see, as T<sub>R</sub>S express other prosurvival factors. However, recent data

demonstrating continuous recruitment of T<sub>R</sub>S to VAT via the circulation led us to assess potential differences in the migration of cells (Vasanthakumar et al., 2020).

In both intact and mixed bone marrow chimeric mice, YF and KO splenic T<sub>R</sub>S contained a small but significantly increased population of ST2<sup>+</sup> T<sub>R</sub>S (Fig. 8, A and B), a subset of T<sub>R</sub>S that is both transcriptionally and epigenetically poised to take up residence in peripheral tissues (Delacher et al., 2017; Delacher et al., 2020). Given this, we hypothesized that superior migration and accumulation could account for the increased frequency of VAT-T<sub>R</sub>S in YF and KO mice. Although CCR2 facilitates recruitment of T<sub>R</sub>S to VAT (Vasanthakumar et al., 2020), we detected no difference in CCR2 expression among genotypes and a modest decrease in CCR2<sup>+</sup> T<sub>R</sub>S in KO spleens (Fig. S5 A), arguing against enhanced CCR2-mediated recruitment of YF and KO T<sub>R</sub>S to VAT.

Previous studies identified an open chromatin landscape around the *Ccr3* locus as well as high *Ccr3* transcript levels in VAT-T<sub>R</sub>S (Cipolletta et al., 2012; Li et al., 2018). The frequency of CCR3-expressing splenic T<sub>R</sub>S was slightly elevated in both young ( $\leq 8$  wk) and older ( $> 8$  wk) YF and KO mice (Fig. S5 B), indicating the presence of a T<sub>R</sub> population primed for both potential early seeding and continuous repopulation of peripheral tissues. In line with this, YF and KO VAT contained more CCR3<sup>+</sup> T<sub>R</sub>S compared with WT mice, and this population increased with age (Fig. 8 C). In mixed bone marrow chimeras, a significantly greater frequency of YF and KO donor T<sub>R</sub>S were CCR3<sup>+</sup> in spleen and VAT (Fig. S5 C). Additionally, YF and KO VAT contained a unique population of T<sub>R</sub>S that expressed CCR3 alone, while WT VAT-T<sub>R</sub>S expressing CCR3 were also positive for CCR2 (Fig. 8 D). CCR3 expression was unique to VAT-T<sub>R</sub>S, unlike CCR2, which we found to be also highly expressed on VAT-T<sub>eff</sub>S (Fig. 8 C). Additionally, the accumulation of CCR3<sup>+</sup> T<sub>R</sub>S was unique to VAT, as we detected very little CCR3 expression in skin, lungs, and large intestine T<sub>R</sub>S, and no differences across genotypes (Fig. S5, D and E). We detected substantial expression of the CCR3 ligands *Ccl11* and *Ccl24* in the VAT, with no differences detected either by age or genotype and little expression of *Ccl5*, *Ccl7*, and *Ccl26* (Fig. 8 E).

To determine if ICOS signaling could directly impact expression of CCR3 on T<sub>R</sub>S, WT, YF, and KO VAT-CD4<sup>+</sup> cells were cultured with  $\alpha$ CD3/ $\alpha$ CD28 in the presence or absence of an agonistic  $\alpha$ ICOS Ab (Fig. 8 F). We additionally added 500 U/ml IL-2 to all conditions to account for any deficiencies in IL-2 production by YF and KO VAT-T<sub>eff</sub>S. After 48 h in culture, T<sub>R</sub> frequency remained unchanged in both groups. However, the frequency of CCR3<sup>+</sup> T<sub>R</sub>S in WT cultures significantly decreased after 2 d with addition of an ICOS agonist, whereas no changes

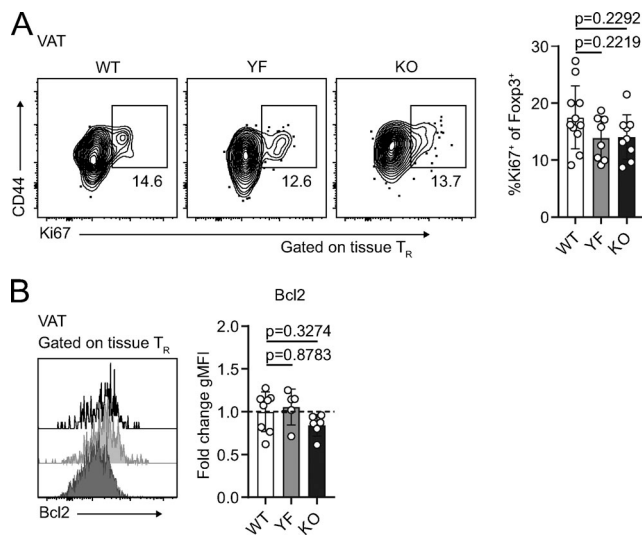


**Figure 7. Increased abundance of YF and KO VAT-T<sub>R</sub> is not due to enhanced proliferation or Bcl2 expression.** **(A and B)** Ki67 (%), **(A)** and Bcl2 (gMFI) expression **(B)** in tissue-localized VAT-T<sub>R</sub>S as measured by flow cytometry directly ex vivo. Bcl2 gMFI was calculated as fold change compared with average expression in WT T<sub>R</sub>S for each individual experiment. Dashed line in B marks average value of WT control samples (Ki67:  $n = 3-5$  per group from three independent experiments; Bcl-2:  $n = 3-5$  per group from two independent experiments). Mice were age matched within independent experiments, and pooled data are from experiments using male mice aged 8–16 wk. Statistical significance was determined using one-way ANOVA with Tukey's post-test. All data are presented as mean values  $\pm$  SD.

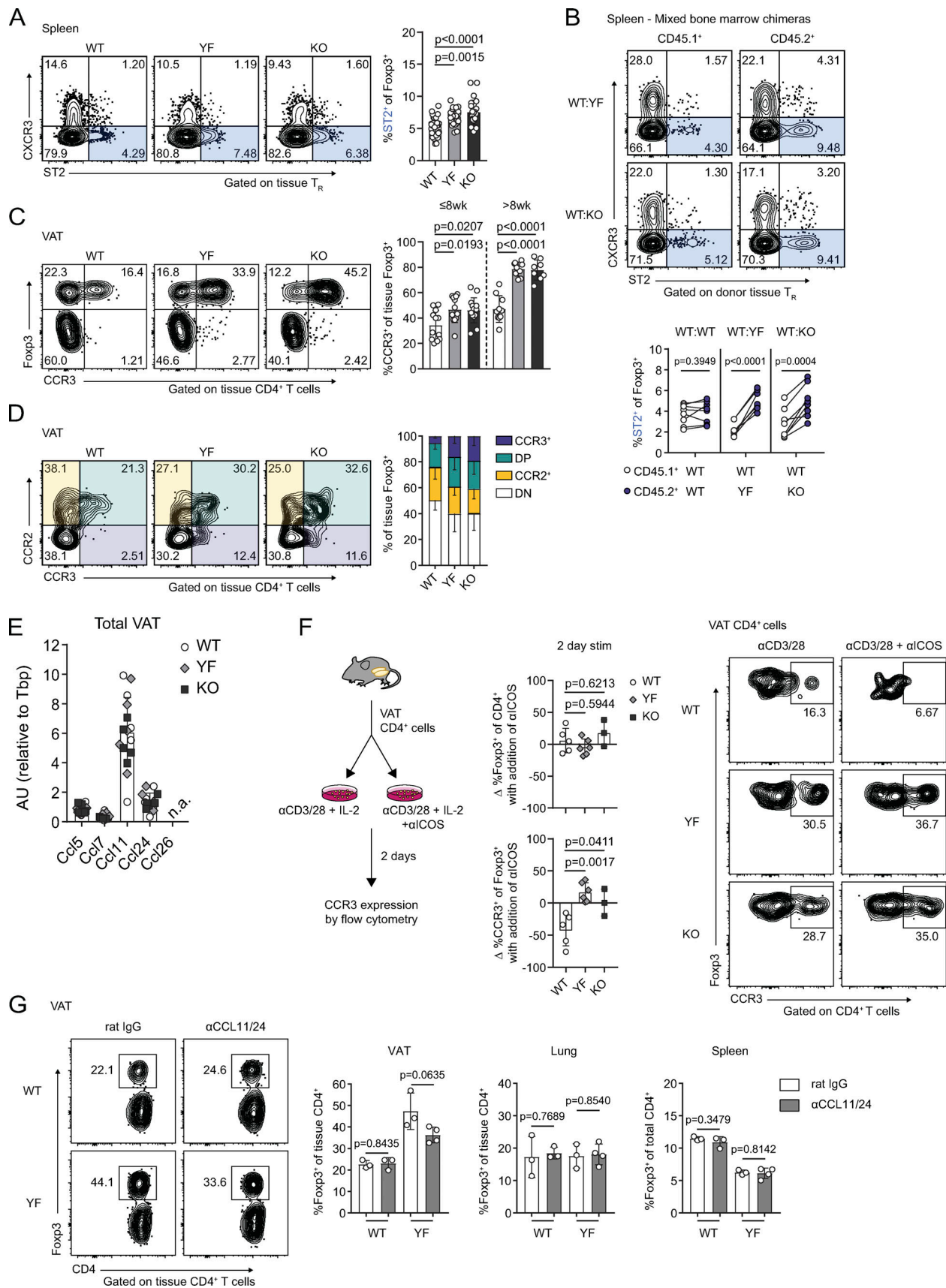


Figure 8. **Increased VAT-T<sub>R</sub> accumulation in the absence of ICOS signaling is associated with elevated CCR3 expression.** (A) ST2 expression in splenic T<sub>RS</sub> (n = 3–5 per group from eight independent experiments). (B) ST2 expression in CD45.1<sup>+</sup> and CD45.2<sup>+</sup> donor splenic T<sub>RS</sub> in WT:YF and WT:KO chimeric mice.

Lines connect CD45.1<sup>+</sup> and CD45.2<sup>+</sup> donor splenic T<sub>R</sub>S within the same chimera ( $n = 3-5$  chimeric mice per group from three independent experiments). **(C)** Expression of CCR3 in VAT-T<sub>R</sub>S in mice  $\leq 8$  wk and  $>8$  wk of age ( $n = 3-5$  per group from seven independent experiments). **(D)** Expression of CCR2 and CCR3 by VAT-T<sub>R</sub>S ( $n = 3-5$  per group from two independent experiments). DP, CCR2<sup>+</sup>CCR3<sup>+</sup>; DN, CCR2<sup>-</sup>CCR3<sup>-</sup>. **(E)** Expression of indicated CCR3 ligands in total VAT normalized to *Tbp* as measured by qPCR (n.d. indicates not detected;  $n = 5$  per group). **(F)** Schematic of in vitro culture experiments examining the impact of ICOS signaling on CCR3 expression (left). Graphs indicating fold change in T<sub>R</sub> frequency of CD4<sup>+</sup> cells and %CCR3<sup>+</sup> of T<sub>R</sub>S between individual culture samples stimulated (stim) with or without  $\alpha$ ICOS for 2 d (middle). Representative flow cytometry plots with frequency of CCR3<sup>+</sup> T<sub>R</sub>S after 2 d in specified culture conditions (right;  $n = 1-3$  per group from three independent experiments). **(G)** Left: Representative flow cytometry plots indicating VAT-T<sub>R</sub> frequency with or without CCL11/24 blockade. Graphs summarize T<sub>R</sub> frequencies in indicated tissues after 2 wk ( $n = 3-4$  per group). Mice were age matched within independent experiments and collectively; pooled data are from experiments using male mice aged 8–16 wk unless otherwise indicated. Statistical significance was determined using one-way ANOVA with Tukey's post-test (A and C); two-tailed, paired Student's *t* test for expression in donor cells within the same chimeric mouse (B); and two-tailed Student's *t* test (F and G). All data are presented as mean values  $\pm$  SD.

were observed in YF or KO cultures, indicating that ICOS-dependent PI3K signaling can directly antagonize CCR3 expression in T<sub>R</sub>S (Fig. 8 F).

To address the impact of CCR3 signaling on continuous T<sub>R</sub> seeding of VAT in vivo, we administered blocking antibodies to the CCR3 ligands CCL11 and CCL24 to 8–10-wk-old WT and YF mice. Blockade of CCL11/24 for  $\sim 2$  wk resulted in a modest, although not statistically significant, decrease in the frequency of VAT-T<sub>R</sub>S specifically in YF mice, with no differences in T<sub>R</sub> abundance in spleen or lungs between treated and untreated mice (Fig. 8 G). We additionally noted a slight reduction in VAT eosinophils in YF mice treated with  $\alpha$ CCL11/24 (Fig. S5 F). Together, these results suggest a potential mechanism by which loss of ICOS-dependent PI3K signaling can drive increased recruitment of T<sub>R</sub>S to VAT by CCR3-CCL11/24 interactions.

## Discussion

We have identified surprising tissue-specific effects of ICOS signaling on T<sub>R</sub> abundance and phenotype. Although there was a significant loss of CD44<sup>+</sup> eT<sub>R</sub>S in the spleen, pLN, skin, and lungs of YF and KO mice compared with WT, there was a substantial increase in T<sub>R</sub> abundance in VAT. T<sub>R</sub> frequency and phenotype were similar in YF and KO mice, including comparably altered readouts of PI3K signaling, suggesting that ICOS primarily impacts T<sub>R</sub> abundance and homeostasis via PI3K-dependent mechanisms.

In addition to supporting VAT-T<sub>R</sub> abundance, loss of ICOS signaling promoted a highly suppressive VAT-T<sub>R</sub> phenotype, including an increased proportion of T<sub>R</sub>S expressing KLRG1, CD69, and IL-10. In vitro, addition of ICOS stimulation augments IL-10 production in CD4<sup>+</sup> T cells, while loss of ICOS signaling in vivo results in reduced T<sub>R</sub> abundance and IL-10 expression in models of autoimmunity, allergy, and infection (Busse et al., 2012; Hutloff et al., 1999; Kohyama et al., 2004; Kornete et al., 2012; Landuyt et al., 2019; Redpath et al., 2013). Although ICOS expression is associated with IL-10-producing T<sub>R</sub>S, ICOS signaling does not appear to be intrinsically required for IL-10 production. CD4<sup>+</sup> T cells from KO mice are capable of producing WT levels of IL-10 in vitro and, interestingly, appear to produce more IL-10 than WT counterparts under Th2-polarizing conditions (Dong et al., 2001). Furthermore, recent studies assessing T<sub>R</sub>S in the brain during chronic *Toxoplasma gondii* infection and lamina propria T<sub>R</sub>S at baseline report no changes in IL-10 production in the presence or absence of ICOS signaling (Landuyt

et al., 2019; O'Brien et al., 2019). Therefore, the reduction in IL-10<sup>+</sup> T<sub>R</sub>S with ICOS blockade observed in specific in vivo models is likely due to insufficient activation or access to specific environmental cues within tissues rather than an inherent requirement for ICOS signaling to drive IL-10 production.

VAT is a complex tissue, consisting of triglyceride-containing adipocytes and a variety of immune cells that function to maintain metabolic homeostasis. In YF and KO mice, other immune cells in addition to T<sub>R</sub>S showed evidence of an anti-inflammatory phenotype. Although ATM and VAT-ILC2 abundance was similar across genotypes at baseline, eosinophil frequency was significantly elevated in YF and KO VAT. In YF and KO mice, VAT-T<sub>eff</sub>S were skewed toward a Th2 phenotype in a cell-intrinsic manner, with an increased frequency of ST2-expressing and IL-10-producing cells. Therefore, in addition to promoting an anti-inflammatory state by sustaining VAT-T<sub>R</sub>S, global loss of ICOS signaling supports the abundance and phenotype of other anti-inflammatory adipose-resident immune cells. These combined changes in cellular composition in VAT in the absence of ICOS signaling were maintained in the setting of a long-term HFD and rendered YF and KO mice more resistant to HFD-induced loss of insulin sensitivity. Changes in insulin responsiveness were subtle, despite a significant increase in T<sub>R</sub>S in YF and KO mice. A recent study demonstrated that ablation of IL-10 improved insulin sensitivity in mice (Rajbhandari et al., 2018). Thus, it is possible that the increased IL-10 production we observed in VAT-T<sub>R</sub>S and VAT-T<sub>eff</sub>S in the absence of ICOS signaling offsets the insulin-sensitizing effects of increased VAT-T<sub>R</sub> abundance in these mice.

YF and KO donor T<sub>R</sub>S preferentially repopulated VAT in mixed bone marrow chimeras and were able to outcompete both donor and endogenous WT T<sub>R</sub>S. ST2 is expressed on a large fraction of VAT-T<sub>R</sub>S (Vasanthakumar et al., 2015), and although the frequency of ST2-expressing VAT-T<sub>R</sub>S was not changed in intact mice, YF and KO VAT-T<sub>R</sub>S in mixed bone marrow chimeras were composed of significantly more ST2<sup>+</sup> cells compared with WT donor T<sub>R</sub>S, suggesting that the competitive advantage of YF and KO donor T<sub>R</sub>S in chimeric VAT is in part due to an enhanced ability to access available IL-33 through increased ST2 expression. The transcriptional regulators BATF and IRF4 cooperate to induce expression of ST2 in T<sub>R</sub>S, possibly downstream of TCR signals as well as through IL-33 signaling itself (Vasanthakumar et al., 2015). Additionally, IL-2 can work synergistically with IL-33 to up-regulate ST2 and specifically expand ST2<sup>+</sup> T<sub>R</sub>S (Guo et al., 2009; Matta et al., 2014). T<sub>R</sub>S are unable to produce IL-2 themselves due to Foxp3-mediated

transcriptional repression at the *Il2* locus (Wu et al., 2006; Ono et al., 2007) and therefore are dependent on paracrine sources of IL-2 produced by, for example, autoreactive T<sub>eff</sub>S (Setoguchi et al., 2005; Stolley and Campbell, 2016). However, KO T<sub>eff</sub>S are defective in production of IL-2 compared with T<sub>eff</sub>S from WT mice (Dong et al., 2001). The absence of an enriched population of ST2-expressing YF and KO VAT-T<sub>R</sub>S at baseline may be explained by this lack of IL-2, which is rescued in the presence of WT IL-2-producing cells in mixed bone marrow chimeras.

Molofsky et al. (2015) have argued that IL-33 signaling on T<sub>R</sub>S in VAT is mediated through ICOS/ICOSL interactions with ILC2s and that absence of this interaction results in loss of VAT-T<sub>R</sub>S. In their system, blockade of ICOS signaling was assessed in *Icosl*<sup>-/-</sup> mice. Consistent with their data in *Icosl*<sup>-/-</sup> mice, we did not observe any differences in ILC2 frequency or number in VAT of KO or YF mice. However, given that ILC2s express both ICOS and ICOSL, loss of one versus the other could differentially impact ILC2 function, resulting in unique cell-extrinsic impacts on T<sub>R</sub>S. Additionally, recent work revealed ligand-independent, constitutive ICOS signaling through PI3K-dependent pathways, which relies on p85 association with the ICOS cytoplasmic YMFM motif and interactions between the ICOS transmembrane domain and the tyrosine kinase Lck (Feito et al., 2003; Wan et al., 2020). Thus, the reported differences observed in our study and Molofsky's may be the result of low-level, cell-intrinsic PI3K activation in ICOS-expressing T<sub>R</sub>S from *Icosl*<sup>-/-</sup> mice.

Although CCR2 plays an important role in recruitment of T<sub>R</sub>S to VAT, we did not detect any differences in CCR2 expression in the absence of ICOS signaling. However, the frequency of CCR3<sup>+</sup> T<sub>R</sub>S was increased in the spleen and VAT of YF and KO mice, which was due to cell-intrinsic loss of ICOS signaling and was enhanced with age. CCR3 is primarily associated with type 2 responses (Danilova et al., 2015; Francis et al., 2007; Humbles et al., 2002; Ma et al., 2002; Nagakubo et al., 2016), and lean, metabolically healthy VAT is maintained in an anti-inflammatory state by the presence of Th2-associated cells. In vivo blockade of CCL11/24 resulted in a modest reduction of T<sub>R</sub>S in YF VAT with no changes in other tissues analyzed. Parabiosis experiments demonstrated recruitment of circulating parabiont-derived T<sub>R</sub>S to VAT after months of shared circulation (Kolodin et al., 2015; Vasanthakumar et al., 2020), indicating that recruitment of T<sub>R</sub>S to VAT occurs throughout adulthood. Thus, longer-term Ab-mediated blockade may be necessary to observe significant effects on T<sub>R</sub> accumulation in our system. Additionally, addressing the role of CCR3 is further complicated by its promiscuity, and whether compensation through other ligands occurs during in vivo blockade is unknown. In vitro, we found that ICOS stimulation resulted in reduced CCR3 expression in WT VAT-T<sub>R</sub>S, with no changes in YF or KO cultures, suggesting that ICOS-dependent PI3K signaling inhibits expression of CCR3. Control of CCR3 expression in T cells has not been extensively characterized; however, there is evidence that the transcription factor GATA3 is able to bind to a regulatory region in the *Ccr3* locus (Kong et al., 2013). Nonlymphoid T<sub>R</sub>S, including VAT-T<sub>R</sub>S, express high levels of GATA3 (Cipolletta et al., 2012; Delacher et al., 2020). However, whether ICOS signaling impacts CCR3 expression by modulating GATA3 expression or activity and

whether GATA3 is involved in controlling CCR3 expression in T<sub>R</sub>S remain to be explored.

Most studies assessing VAT-T<sub>R</sub> biology use older male mice due to an increased abundance of canonical VAT-T<sub>R</sub>S with age (Cipolletta et al., 2015). However, mediators of tissue inflammation, including IL-6, TNF $\alpha$ , and IL1 $\beta$ , are up-regulated in the VAT of aged male mice (older than 24 wk; Wu et al., 2007). We observed consistent accumulation of VAT-T<sub>R</sub>S from 5 wk on in all three genotypes, which was correlated with an increase in CCR3<sup>+</sup> T<sub>R</sub>S up to ~20 wk of age. CCR2 regulates T cell access to sites of inflammation (Lee et al., 2007), and studies assessing the contribution of CCR2 on T<sub>R</sub> migration to VAT use mice aged 25–30 wk, when measures of VAT inflammation are increasing. CCR2 and CCR3 likely both have important roles for promoting recruitment of T<sub>R</sub>S to VAT; however, it will be necessary to evaluate whether these receptors are used differentially based on age, sex, and inflammation. For example, CCR3 may be one important factor for early seeding and continuous recruitment of T<sub>R</sub>S to VAT in comparatively younger mice when VAT inflammation is low. With increasing age and inflammation (particularly in male mice), a switch to CCL2-CCR2-mediated migration may dominate.

Future studies are required to understand how ICOS exerts tissue-specific effects. The skin and lungs are under chronic stimulation by environmental antigens and commensal microbes, whereas the sterile VAT is maintained in a Th2-skewed environment in metabolically healthy mice. The milieu of chemokines and cytokines expressed at baseline in these tissues is likely very different. Indeed, T<sub>R</sub>S express distinct patterns of homing receptors and adhesion molecules to appropriately access specific nonlymphoid tissues (reviewed in Campbell and Koch, 2011). Absence of ICOS signaling may support expression of chemokine receptors that preferentially drive T<sub>R</sub>S to VAT due to constitutive expression of unique chemokines within this tissue. Additionally, VAT-T<sub>R</sub>S may rely less on PI3K signals than T<sub>R</sub>S found from other tissues, due to the presence of other supporting factors in the VAT of naive mice, such as high levels of IL-33. Indeed, a recent study demonstrated that insulin receptor deletion in T<sub>R</sub>S, which also results in reduced PI3K signaling, led to an increased suppressive phenotype in VAT-T<sub>R</sub>S and enhanced insulin sensitivity (Wu et al., 2020).

We describe a surprising, antagonistic role for ICOS-dependent PI3K signaling in the accumulation, prototypical phenotype, and function of T<sub>R</sub>S specifically in VAT. We suggest that absence of ICOS signaling supports enhanced recruitment of T<sub>R</sub>S to VAT associated with increased expression of CCR3. Further studies will be needed to identify the molecular mechanisms by which ICOS inhibits the VAT-T<sub>R</sub> phenotype and CCR3 expression. This highlights the complexity of tissue-specific T<sub>R</sub> development and accumulation and the importance of considering how signals from the immune environment elicit both cell- and tissue-specific effects.

## Materials and methods

### Mice

CD45.1<sup>+</sup> B6.SJL (B6.SJL-PtprcaPepcb/BoyJ), B6.*Icos*<sup>-/-</sup> (B6.129P2-*Icostm1Mak/J*), and B6.*Foxp3mRFP* (C57BL/6-*Foxp3tm1Flv/J*) mice

were purchased from The Jackson Laboratory. B6.*IcosY181F* mice were provided by M. Pepper (University of Washington, Seattle, WA). All mice were backcrossed to a C57BL/6J background for at least 10 generations. *Foxp3mRFP* mice were used as WT controls, and mice from different genotypes used were cohoused at weaning. CD45.1<sup>+</sup> B6.SJL mice were crossed to B6.*Foxp3mRFP* mice to generate *Foxp3mRFP* mice expressing CD45.1, CD45.2, and CD45.1/2 allelic variants. B6.*Icos*<sup>-/-</sup> and B6.*IcosY181F* mice were crossed to B6.*Foxp3mRFP* mice to generate B6.*Icos*<sup>-/-</sup> and B6.*IcosY181F* mice expressing *Foxp3mRFP*. All animals were bred and housed in specific pathogen-free conditions under the approval of the Institutional Animal Care and Use Committee of the Benaroya Research Institute. Males were used unless specified otherwise. Age of mice is indicated per experiment.

### Mixed bone marrow chimeras

Bone marrow cells were prepared from donor mice by flushing femurs and tibias with PBS. RBCs from filtered cells were lysed in ammonium-chloride-potassium lysis buffer (Life Technologies) for 5 min at room temperature (RT). Recipient mice were lethally irradiated (2 × 600 rad separated by ≥4 h). Mixed bone marrow chimeras were generated by retro-orbitally injecting a 1:1 ratio (≥2 × 10<sup>6</sup> total cells) of bone marrow cells of the appropriate genotypes into anesthetized recipient mice. Chimeric mice were rested for ≥10 wk.

### Intravascular labeling

Mice were anesthetized with 4% isoflurane, and 3 μg BV510- or BV650-conjugated CD45 (30-F11) was injected into mice retro-orbitally in 200 μl PBS 5 min before sacrifice. Single-cell suspensions were prepared for flow cytometry as described below, and localization of cells was determined by positive (blood-exposed) and negative (tissue-restricted) staining.

### Cell isolation

Single-cell suspensions were prepared from spleen and pLNs (pooled inguinal, axillary, brachial, and superficial cervical nodes) by tissue disruption with frosted glass slides into RPMI with 10% bovine calf serum (BCS; R-10) and filtered through nitex mesh. Blood was collected via cardiac puncture into PBS containing 2 mM EDTA. Epididymal VAT and inguinal SQAT were excised, finely minced with scissors, and digested in RPMI basal medium with 0.14 U/ml Liberase (Roche) and 10 U/ml DNase I (Roche) for 30 min at 37°C with shaking (200 rpm). Supernatants were filtered through a 100-μm cell strainer and washed several times to remove mature adipocytes from the stromal vascular fraction. Ears were harvested for skin-infiltrating cells. Dorsal and ventral sides were separated using forceps and digested as described for VAT/SQAT for 45 min. Lungs were digested as described for skin. Large intestines were cleaned, stripped of fatty tissue, and inverted. Tissue was placed into extraction media (RPMI basal medium, 2 mM dithiothreitol, 1 mM EDTA, and 2% BCS) and shaken at 37°C for 20 min to release intraepithelial lymphocytes (IELs). IEL-containing supernatant was removed and filtered into 50-ml conical tubes. For lamina propria lymphocyte isolation immediately following incubation with extraction media, tissue was finely minced and placed into digestion media (RPMI basal media, 300 U/ml

collagenase I [Worthington Biochemical Corporation], and 1% BCS), shaken for 30 min at 37°C, and filtered into 50-ml conical tubes. Isolated cells from all tissues were incubated in ammonium-chloride-potassium lysis buffer for 5 min, washed with R-10, and stained for flow cytometry or cultured for intracellular cytokine or chemokine receptor staining.

### Flow cytometry and intracellular cytokine staining

Single-cell suspensions were stained with Fixable Viability Dye eFluor 780 (eBioscience) in PBS for 10 min at RT. For surface staining, cells were incubated at 4°C for 30 min in FACS buffer (PBS, 2% BCS) with directly conjugated Abs for murine proteins. Abs were purchased from BioLegend unless noted: CD4 (RM4-5), CD8 (53-6.7), CD11b (M1/70), CD11c (N418), CD25 (PC61), CD44 (IM7), CD45 (30-F11), CD45.1 (A20), CD45.2 (104), CD62L (MEL-14), CD69 (H1.2F3), CD206 (C068C2), CXCR3 (CXCR3-173), F4/80 (BM8), Gr1 (RB6-8C5), ICOS (15F9), KLRG1 (2F1/KLRG1), Siglec-F (E50-2440; BD Biosciences), ST2 (U29-93; BD Biosciences), and TCRβ (H57-597). For intracellular staining, cells were stained for surface antigens as described above, washed, and permeabilized for 20 min with eBioscience Fix/Perm buffer at 4°C. Cells were washed and stained in PermWash buffer (eBioscience) for 30 min at 4°C with Abs (purchased from BioLegend unless noted) against Bcl2 (BCL10C4), CTLA-4 (UC10-4B9), Foxp3 (FJK-16s; Invitrogen), IFN-γ (XMG1.2; BD Biosciences), IL-10 (JES5-16E3), Ki67 (11F6), and TNFα (MP6-XT22). For intracellular cytokine staining following restimulation, cells were incubated in FACS tubes with PMA (50 ng/ml) and ionomycin (1 μg/ml) plus monensin (2 μM) in 0.3 ml complete RPMI medium (RPMI with 10% [vol/vol] fetal bovine serum, 100 U/ml penicillin, 100 μg/ml streptomycin, 25 μg/ml gentamycin, 1 mM sodium pyruvate, 10 mM Hepes, 2 mM L-glutamine, and 55 μM β-ME) for 4 h at 37°C, 5% CO<sub>2</sub> before staining as described above. Loss of monomeric RFP expression occurred with our fixation/permeabilization protocols, requiring intracellular Foxp3 staining. Data were acquired on LSR II or FACSCanto flow cytometers (BD Biosciences) and analyzed using FlowJo software (TreeStar). Due to intraexperimental variability, geometric mean fluorescence intensity (gMFI) was normalized as fold change compared with average expression in WT samples per experiment. Polybead polystyrene nonfluorescent microspheres (15 mm; Polysciences) were used to determine absolute cell numbers in flow cytometry samples. 100 μl of a fixed concentration (C<sub>B</sub>) of beads was mixed with 100 μl cells to be counted. Samples were acquired on a flow cytometer, with gates drawn on lymphocyte and bead populations based on their forward- and side-scatter properties. The ratio of lymphocyte gate events (N<sub>L</sub>) to bead gate events (N<sub>B</sub>) was determined and used to calculate the concentration (C<sub>L</sub>) of the original cell suspension as follows: C<sub>L</sub> = (N<sub>L</sub>/N<sub>B</sub>) × C<sub>B</sub>.

### Phospho-flow cytometry staining

Approximately one fourth of each spleen was immediately disrupted between frosted glass slides into BD Fix/Perm buffer (BD Biosciences). Cells were incubated for 20 min at RT, washed in FACS buffer, and resuspended in 90% ice-cold methanol for ≥30 min. Cells were washed with BD Perm/Wash buffer (BD Biosciences) and stained for surface and intracellular antigens,

including p-S6 (D57.2.2E; Cell Signaling Technology), for 45 min at RT.

### Chemokine receptor staining

Freshly isolated cells were incubated for 2.5 h at 37°C, 5% CO<sub>2</sub> in RPMI-C. For CCR7 expression, cells were incubated with CCL19-human IgGfc fusion protein for 20 min at 4°C, washed, and then incubated with PE-conjugated goat anti-human IgGfc (Jackson ImmunoResearch Laboratories) for 20 min at 4°C. To detect CCR2 (475301; R&D Systems) and CCR3 (J073E5; BioLegend), cells were incubated for 30 min at 37°C with directly conjugated antibodies diluted in FACS buffer. Cells were washed twice with FACS buffer before being acquired on the flow cytometer.

### Histology

VAT was excised, immediately fixed in 10% formalin for 24 h, and then paraffin embedded. H&E staining was performed on 6- $\mu$ m tissue sections by the Benaroya Research Institute Histology Core. Slides were imaged at RT with a Leica DM E brightfield microscope with a 10 $\times$  eyepiece and 20 $\times$  objective lens (together, 200 $\times$ ). Images were captured with a Leica EC3 3.1 megapixel digital color camera and imported into Leica Application Suite EZ imaging software.

### RNA extraction and quantitative PCR (qPCR)

VAT was dissected, immediately stabilized in RNAlater (Thermo Fisher), and frozen at -20°C until ready for processing. ~100 mg tissue was homogenized in 1 ml Qiazol, and RNA was extracted using RNeasy Lipid Tissue Mini Kit (Qiagen) according to the manufacturer's instructions. RNA quality and quantity were determined using an ND-1000 spectrophotometer (NanoDrop; Thermo Fisher). 500 ng template RNA was reverse transcribed with random hexamer primers in 20  $\mu$ l using the RevertAid First Strand cDNA Synthesis Kit (Thermo Fisher) and subsequently diluted 1:3.3 with nuclease-free water. qPCR was performed using 2  $\mu$ l diluted cDNA and presynthesized TaqMan Gene Expression assays in TaqMan Gene Expression Master Mix (Applied Biosystems) for amplification of the following transcripts in a final volume of 20  $\mu$ l: *Ccl5* (Mm01302427\_m1), *Ccl7* (Mm00443113\_m1), *Ccl11* (Mm0441238\_m1), *Ccl24* (Mm00444701\_m1), and *Ccl26* (Mm02763057\_u1). Samples were run in technical triplicates using the QuantStudio 5 Real-Time PCR System (Thermo Fisher) with 10-min initial activation at 95°C followed by 40 cycles of 15 s at 95°C, 60 s at 60°C. Mean target mRNA levels were calculated by the  $\Delta\Delta$ CT method and normalized to *Tbp* (Mm01277042\_m1) expression using QuantStudio Design and Analysis Software (Thermo Fisher).

### In vitro stimulation of VAT T cells

VAT was pooled from two or three mice of the same genotype to ensure adequate cell number for culture. Cells were isolated as described above, and CD4<sup>+</sup> T cells were enriched by incubating cells with CD4 MicroBeads and positively selecting with MACS cell separation MS columns (Miltenyi Biotec). Purified cells were resuspended in RPMI-C with 500 U/ml recombinant IL-2 (eBioscience). Cells were cultured for 48 h in 96-well flat-bottom plates with plate-bound  $\alpha$ CD3 (2C11) and  $\alpha$ CD28 (37.51) from Bio X Cell at 1  $\mu$ g/ $\mu$ l, with or without the addition of plate-

bound  $\alpha$ ICOS (C398.4A; BioLegend) at 2  $\mu$ g/ $\mu$ l. Expression of CCR3 was assessed by flow cytometry as described above.

### Rapamycin treatment

Mice were given rapamycin (1 mg/kg) three times per week for 3 wk by i.p. injection in PBS containing 5.2% PEG-400, 5.2% Tween 80, and 0.5% ethanol. Control animals were given vehicle only. Mice were euthanized for analysis of T<sub>R</sub> abundance in the spleen and VAT 2 d after the final injection.

### In vivo Ab blockade

Mice aged 8–10 wk were given 0.75  $\mu$ g/g body weight  $\alpha$ CCL11 and  $\alpha$ CCL24 (MAB420 and MAB528; R&D Systems) or an equivalent amount of rat IgG (Sigma) diluted in PBS by i.p. injection on days 0, 5, and 10 and sacrificed for analysis on day 13.

### HFD

Mice were placed on an 18-wk HFD (60% kcal fat diet; Research Diets D124928, ad libitum) beginning at 5–7 wk of age. Weights and BGL by tail prick (Contour Next One glucose meter; Ascensia Diabetes Care) were taken weekly after 6 h of fasting.

### ITT and GTT

ITTs were performed in conscious mice fasted for 6 h. 1 U/kg human insulin (Sigma) was given i.p., and blood was collected by tail prick for BGL at 0, 15, 30, 45, and 60 min after insulin administration. 3 d later, GTTs were performed in conscious mice fasted for 6 h. 1 g/kg glucose (Sigma) was administered i.p. Blood was collected by tail prick for BGL at 0, 15, 30, 60, 90, and 120 min after glucose bolus.

### Statistical analysis

All data are presented as mean values  $\pm$  SD, and graphs were created and analyzed using Prism Software (GraphPad). Comparisons between genotypes were analyzed using one- or two-way ANOVA where appropriate, adjusted for multiple comparisons using Tukey's post-test. For mixed bone marrow chimeras, statistical significance was determined using two-tailed, paired Student's *t* tests when comparing cells within the same chimeric mouse.

### Online supplemental material

Fig. S1 shows ICOS expression across gated splenic T<sub>R</sub> populations and summarizes pLN T<sub>R</sub> frequency. Fig. S2 shows further characterization of splenic and VAT-T<sub>R</sub>s by flow cytometry and the impact of rapamycin treatment on T<sub>R</sub> abundance in the spleen and VAT. Fig. S3 shows VAT histology (H&E staining) and frequencies of ATM and ILC2 populations by flow cytometry. Fig. S4 shows further characterization of mixed bone marrow chimeras. Fig. S5 expands on CCR2 and CCR3 expression in specific tissues in both intact and chimeric mice (flow cytometry) and characterizes eosinophil frequencies in VAT after in vivo CCL11/24 blockade.

### Acknowledgments

We thank A. Wojno, K. Arumuganathan, and T. Nguyen for maintaining the Benaroya Research Institute Flow Cytometry

Core; P. Johnson in the Benaroya Research Institute Histology/Imaging Core; and D. Hackney and S. Zraika from the University of Washington Diabetes Research Center Cell Function Analysis Core for help with metabolic profiling tests. M. Pepper generously provided *IcosY181F* mice with kind permission from W.-K. Suh. A. Burich, C. Toledano, and the Benaroya Research Institute vivarium staff helped maintain mouse colonies. We thank members of the Campbell laboratory for helpful discussion and laboratory support.

This work was supported by the National Institutes of Health (grants R01AI124693 and R01AI136475 to D.J. Campbell) and National Institutes of Health National Institute of Allergy and Infectious Diseases T32 grant AI106677 and National Institute of General Medical Sciences T32 grant GM007270 (to K.L. Mittelsteadt), and the University of Washington Diabetes Research Center Samuel and Althea Stroum Endowed Graduate Fellowship (2P30 DK17047) to K.L. Mittelsteadt.

Author contributions: K.L. Mittelsteadt and D.J. Campbell conceptualized the study and designed experiments. K.L. Mittelsteadt, E.T. Hayes, and D.J. Campbell performed experiments. K.L. Mittelsteadt and D.J. Campbell analyzed data and wrote the manuscript.

Disclosures: The authors declare no competing interests exist.

Submitted: 2 June 2020

Revised: 24 August 2020

Accepted: 15 March 2021

## References

- Ahnstedt, H., M. Roy-O'Reilly, M.S. Szychala, A.S. Mobley, J. Bravo-Alegria, A. Chauhan, J. Aronowski, S.P. Marrelli, and L.D. McCullough. 2018. Sex differences in adipose tissue CD8+ T cells and regulatory T cells in middle-aged mice. *Front. Immunol.* 9:659. <https://doi.org/10.3389/fimmu.2018.00659>
- Ali, N., B. Zirak, R.S. Rodriguez, M.L. Pauli, H.-A. Truong, K. Lai, R. Ahn, K. Corbin, M.M. Lowe, T.C. Scharshmidt, et al. 2017. Regulatory T cells in skin facilitate epithelial stem cell differentiation. *Cell.* 169:1119–1129.e11. <https://doi.org/10.1016/j.cell.2017.05.002>
- Anderson, K.G., K. Mayer-Barber, H. Sung, L. Beura, B.R. James, J.J. Taylor, L. Qunaj, T.S. Griffith, V. Vezys, D.L. Barber, and D. Masopust. 2014. Intravascular staining for discrimination of vascular and tissue leukocytes. *Nat. Protoc.* 9:209–222. <https://doi.org/10.1038/nprot.2014.005>
- Arimura, Y., H. Kato, U. Dianzani, T. Okamoto, S. Kamekura, D. Buonfiglio, T. Miyoshi-Akiyama, T. Uchiyama, and J. Yagi. 2002. A co-stimulatory molecule on activated T cells, H4/ICOS, delivers specific signals in T(h) cells and regulates their responses. *Int. Immunol.* 14:555–566. <https://doi.org/10.1093/intimm/14.5.555>
- Arpaia, N., J.A. Green, B. Molledo, A. Arvey, S. Hemmers, S. Yuan, P.M. Treuting, and A.Y. Rudensky. 2015. A distinct function of regulatory T cells in tissue protection. *Cell.* 162:1078–1089. <https://doi.org/10.1016/j.cell.2015.08.021>
- Burhans, M.S., D.K. Hagman, J.N. Kuzma, K.A. Schmidt, and M. Kratz. 2019. Contribution of adipose tissue inflammation to the development of type 2 diabetes mellitus. *Compr. Physiol.* 9:1–58. <https://doi.org/10.1002/cphy.c170040>
- Burmeister, Y., T. Lischke, A.C. Dahler, H.W. Mages, K.-P.P. Lam, A.J. Coyle, R.A. Kroccek, and A. Hutloff. 2008. ICOS controls the pool size of effector-memory and regulatory T cells. *J. Immunol.* 180:774–782. <https://doi.org/10.4049/jimmunol.180.2.774>
- Burzyn, D., W. Kuswanto, D. Kolodin, J.L. Shadrach, M. Cerletti, Y. Jang, E. Sefik, T.G. Tan, A.J. Wagers, C. Benoist, and D. Mathis. 2013. A special population of regulatory T cells potentiates muscle repair. *Cell.* 155:1282–1295. <https://doi.org/10.1016/j.cell.2013.10.054>
- Busse, M., M. Krech, A. Meyer-Bahlburg, C. Hennig, and G. Hansen. 2012. ICOS mediates the generation and function of CD4+CD25+Foxp3+ regulatory T cells conveying respiratory tolerance. *J. Immunol.* 189:1975–1982. <https://doi.org/10.4049/jimmunol.1103581>
- Campbell, D.J. 2015. Control of regulatory T cell migration, function, and homeostasis. *J. Immunol.* 195:2507–2513. <https://doi.org/10.4049/jimmunol.1500801>
- Campbell, D.J., and M.A. Koch. 2011. Phenotypical and functional specialization of FOXP3+ regulatory T cells. *Nat. Rev. Immunol.* 11:119–130. <https://doi.org/10.1038/nri2916>
- Cipolletta, D., M. Feuerer, A. Li, N. Kamei, J. Lee, S.E. Shoelson, C. Benoist, and D. Mathis. 2012. PPAR-γ is a major driver of the accumulation and phenotype of adipose tissue Treg cells. *Nature.* 486:549–553. <https://doi.org/10.1038/nature11132>
- Cipolletta, D., P. Cohen, B.M. Spiegelman, C. Benoist, and D. Mathis. 2015. Appearance and disappearance of the mRNA signature characteristic of Treg cells in visceral adipose tissue: age, diet, and PPARγ effects. *Proc. Natl. Acad. Sci. USA.* 112:482–487. <https://doi.org/10.1073/pnas.1423486112>
- Cretney, E., A. Xin, W. Shi, M. Minnich, F. Masson, M. Miasari, G.T. Belz, G.K. Smyth, M. Busslinger, S.L. Nutt, and A. Kallies. 2011. The transcription factors Blimp-1 and IRF4 jointly control the differentiation and function of effector regulatory T cells. *Nat. Immunol.* 12:304–311. <https://doi.org/10.1038/ni.2006>
- Danilova, E., I. Skirindo, E. Gran, B.J. Hales, W.A. Smith, J. Jahnsen, F.E. Johansen, F.L. Jahnsen, and E.S. Baekkevold. 2015. A role for CCL28-CCR3 in T-cell homing to the human upper airway mucosa. *Mucosal Immunol.* 8:107–114. <https://doi.org/10.1038/mi.2014.46>
- Deiulis, J., Z. Shah, N. Shah, B. Needleman, D. Mikami, V. Narula, K. Perry, J. Hazey, T. Kampfprath, M. Kollengode, et al. 2011. Visceral adipose inflammation in obesity is associated with critical alterations in regulatory cell numbers. *PLoS One.* 6:e16376. <https://doi.org/10.1371/journal.pone.0016376>
- Delacher, M., C.D. Imbusch, D. Weichenhan, A. Breiling, A. Hotz-Wagenblatt, U. Träger, A.-C. Hofer, D. Kägebein, Q. Wang, F. Frauhammer, et al. 2017. Genome-wide DNA-methylation landscape defines specialization of regulatory T cells in tissues. *Nat. Immunol.* 18:1160–1172. <https://doi.org/10.1038/ni.3799>
- Delacher, M., C.D. Imbusch, A. Hotz-Wagenblatt, J.-P. Mallm, K. Bauer, M. Simon, D. Riegel, A.F. Rendeiro, S. Bittner, L. Sanderink, et al. 2020. Precursors for nonlymphoid-tissue Treg cells reside in secondary lymphoid organs and are programmed by the transcription factor BATF. *Immunity.* 52:295–312.e11. <https://doi.org/10.1016/j.immuni.2019.12.002>
- DiSpirito, J.R., D. Zemmour, D. Ramanan, J. Cho, R. Zilionis, A.M. Klein, C. Benoist, and D. Mathis. 2018. Molecular diversification of regulatory T cells in nonlymphoid tissues. *Sci. Immunol.* 3:eaat5861. <https://doi.org/10.1126/sciimmunol.aat5861>
- Dominguez-Villar, M., and D.A. Hafler. 2018. Regulatory T cells in autoimmune disease. *Nat. Immunol.* 19:665–673. <https://doi.org/10.1038/s41590-018-0120-4>
- Dong, C., A.E. Juedes, U.A. Temann, S. Shrestha, J.P. Allison, N.H. Ruddle, and R.A. Flavell. 2001. ICOS co-stimulatory receptor is essential for T-cell activation and function. *Nature.* 409:97–101. <https://doi.org/10.1038/35051100>
- Eller, K., A. Kirsch, A.M. Wolf, S. Sopfer, A. Tagwerker, U. Stanzl, D. Wolf, W. Patsch, A.R. Rosenkranz, and P. Eller. 2011. Potential role of regulatory T cells in reversing obesity-linked insulin resistance and diabetic nephropathy. *Diabetes.* 60:2954–2962. <https://doi.org/10.2337/db11-0358>
- Feito, M.J., R. Vaschetto, G. Criado, A. Sánchez, A. Chiochetti, A. Jiménez-Periáñez, U. Dianzani, P. Portoles, and J.M. Rojo. 2003. Mechanisms of H4/ICOS costimulation: effects on proximal TCR signals and MAP kinase pathways. *Eur. J. Immunol.* 33:204–214. <https://doi.org/10.1002/immu.200390023>
- Feuerer, M., L. Herrero, D. Cipolletta, A. Naaz, J. Wong, A. Nayer, J. Lee, A.B. Goldfine, C. Benoist, S. Shoelson, and D. Mathis. 2009. Lean, but not obese, fat is enriched for a unique population of regulatory T cells that affect metabolic parameters. *Nat. Med.* 15:930–939. <https://doi.org/10.1038/nm.2002>
- Fos, C., A. Salles, V. Lang, F. Carrette, S. Audebert, S. Pastor, M. Ghiotto, D. Olive, G. Bismuth, and J.A. Nunès. 2008. ICOS ligation recruits the p50α PI3K regulatory subunit to the immunological synapse. *J. Immunol.* 181:1969–1977. <https://doi.org/10.4049/jimmunol.181.3.1969>
- Francis, J.N., C.M. Lloyd, I. Sabroe, S.R. Durham, and S.J. Till. 2007. T lymphocytes expressing CCR3 are increased in allergic rhinitis compared with non-allergic controls and following allergen immunotherapy. *Allergy.* 62:59–65. <https://doi.org/10.1111/j.1398-9995.2006.01253.x>

- Gigoux, M., J. Shang, Y. Pak, M. Xu, J. Choe, T.W. Mak, and W.-K.K. Suh. 2009. Inducible costimulator promotes helper T-cell differentiation through phosphoinositide 3-kinase. *Proc. Natl. Acad. Sci. USA*. 106: 20371–20376. <https://doi.org/10.1073/pnas.0911573106>
- Guo, L., G. Wei, J. Zhu, W. Liao, W.J. Leonard, K. Zhao, and W. Paul. 2009. IL-1 family members and STAT activators induce cytokine production by Th2, Th17, and Th1 cells. *Proc. Natl. Acad. Sci. USA*. 106:13463–13468. <https://doi.org/10.1073/pnas.0906988106>
- Han, J.M., D. Wu, H.C. Denroche, Y. Yao, C.B. Verchere, and M.K. Levings. 2015. IL-33 reverses an obesity-induced deficit in visceral adipose tissue ST2+ T regulatory cells and ameliorates adipose tissue inflammation and insulin resistance. *J. Immunol.* 194:4777–4783. <https://doi.org/10.4049/jimmunol.1500020>
- Herman, A.E., G.J. Freeman, D. Mathis, and C. Benoist. 2004. CD4+CD25+ T regulatory cells dependent on ICOS promote regulation of effector cells in the prediabetic lesion. *J. Exp. Med.* 199:1479–1489. <https://doi.org/10.1084/jem.20040179>
- Humbles, A.A., B. Lu, D.S. Friend, S. Okinaga, J. Lora, A. Al-Garawi, T.R. Martin, N.P. Gerard, and C. Gerard. 2002. The murine CCR3 receptor regulates both the role of eosinophils and mast cells in allergen-induced airway inflammation and hyperresponsiveness. *Proc. Natl. Acad. Sci. USA*. 99:1479–1484. <https://doi.org/10.1073/pnas.261462598>
- Hutloff, A., A.M. Dittrich, K.C. Beier, B. Eljaschewitsch, R. Kraft, I. Anagnostopoulos, and R.A. Kroczyk. 1999. ICOS is an inducible T-cell costimulator structurally and functionally related to CD28. *Nature*. 397: 263–266. <https://doi.org/10.1038/16717>
- Ilan, Y., R. Maron, A.-M. Tukupah, T.U. Maioli, G. Murugaiyan, K. Yang, H.Y. Wu, and H.L. Weiner. 2010. Induction of regulatory T cells decreases adipose inflammation and alleviates insulin resistance in ob/ob mice. *Proc. Natl. Acad. Sci. USA*. 107:9765–9770. <https://doi.org/10.1073/pnas.0908771107>
- Kalekar, L.A., J.N. Cohen, N. Prevel, P.M. Sandoval, A.N. Mathur, J.M. Moreau, M.M. Lowe, A. Nosbaum, P.J. Wolters, A. Haemel, et al. 2019. Regulatory T cells in skin are uniquely poised to suppress profibrotic immune responses. *Sci. Immunol.* 4:eaw2910. <https://doi.org/10.1126/sciimmunol.aaw2910>
- Kerdiles, Y.M., D.R. Beisner, R. Tinoco, A.S. Dejean, D.H. Castrillon, R.A. DePinho, and S.M. Hedrick. 2009. Foxo1 links homing and survival of naive T cells by regulating L-selectin, CCR7 and interleukin 7 receptor. *Nat. Immunol.* 10:176–184. <https://doi.org/10.1038/ni.1689>
- Kohyama, M., D. Sugahara, S. Sugiyama, H. Yagita, K. Okumura, and N. Hozumi. 2004. Inducible costimulator-dependent IL-10 production by regulatory T cells specific for self-antigen. *Proc. Natl. Acad. Sci. USA*. 101: 4192–4197. <https://doi.org/10.1073/pnas.0400214101>
- Kolodin, D., N. van Panhuys, C. Li, A.M. Magnuson, D. Cipolletta, C.M. Miller, A. Wagers, R.N. Germain, C. Benoist, and D. Mathis. 2015. Antigen- and cytokine-driven accumulation of regulatory T cells in visceral adipose tissue of lean mice. *Cell Metab.* 21:543–557. <https://doi.org/10.1016/j.cmet.2015.03.005>
- Komatsu, N., and S. Hori. 2007. Full restoration of peripheral Foxp3+ regulatory T cell pool by radioresistant host cells in scurfy bone marrow chimeras. *Proc. Natl. Acad. Sci. USA*. 104:8959–8964. <https://doi.org/10.1073/pnas.0702004104>
- Kong, S.-K.K., B.S. Kim, T.G. Uhm, W. Lee, G.R. Lee, C.-S.S. Park, C.-H.H. Lee, and I.Y. Chung. 2013. Different GATA factors dictate CCR3 transcription in allergic inflammatory cells in a cell type-specific manner. *J. Immunol.* 190:5747–5756. <https://doi.org/10.4049/jimmunol.1203542>
- Kornete, M., E. Sgouroudis, and C.A. Piccirillo. 2012. ICOS-dependent homeostasis and function of Foxp3+ regulatory T cells in islets of nonobese diabetic mice. *J. Immunol.* 188:1064–1074. <https://doi.org/10.4049/jimmunol.1101303>
- Landuyt, A.E., B.J. Klocke, T.B. Colvin, T.R. Schoeb, and C.L. Maynard. 2019. Cutting Edge: ICOS-deficient regulatory T cells display normal induction of Il10 but readily downregulate expression of Foxp3. *J. Immunol.* 202:1039–1044. <https://doi.org/10.4049/jimmunol.1801266>
- Lee, J.H., S.G. Kang, and C.H. Kim. 2007. FoxP3+ T cells undergo conventional first switch to lymphoid tissue homing receptors in thymus but accelerated second switch to nonlymphoid tissue homing receptors in secondary lymphoid tissues. *J. Immunol.* 178:301–311. <https://doi.org/10.4049/jimmunol.178.1.301>
- Levine, A.G., A. Arvey, W. Jin, and A.Y. Rudensky. 2014. Continuous requirement for the TCR in regulatory T cell function. *Nat. Immunol.* 15: 1070–1078. <https://doi.org/10.1038/ni.3004>
- Li, C., J.R. DiSpirito, D. Zemmour, R.G. Spallanzani, W. Kuswanto, C. Benoist, and D. Mathis. 2018. TCR transgenic mice reveal stepwise, multi-site acquisition of the distinctive fat-Treg phenotype. *Cell*. 174:285–299.e12. <https://doi.org/10.1016/j.cell.2018.05.004>
- Luo, C.T., W. Liao, S. Dadi, A. Toure, and M.O. Li. 2016. Graded Foxo1 activity in Treg cells differentiates tumour immunity from spontaneous autoimmunity. *Nature*. 529:532–536. <https://doi.org/10.1038/nature16486>
- Ma, W., P.J. Bryce, A.A. Humbles, D. Laouini, A. Yalcindag, H. Alenius, D.S. Friend, H.C. Oettgen, C. Gerard, and R.S. Geha. 2002. CCR3 is essential for skin eosinophilia and airway hyperresponsiveness in a murine model of allergic skin inflammation. *J. Clin. Invest.* 109:621–628. <https://doi.org/10.1172/JCI0214097>
- Matta, B.M., J.M. Lott, L.R. Mathews, Q. Liu, B.R. Rosborough, B.R. Blazar, and H.R. Turnquist. 2014. IL-33 is an unconventional Alarmin that stimulates IL-2 secretion by dendritic cells to selectively expand IL-33R/ST2+ regulatory T cells. *J. Immunol.* 193:4010–4020. <https://doi.org/10.4049/jimmunol.1400481>
- Miyamoto, K., C.I. Kingsley, X. Zhang, C. Jabs, L. Izikson, R.A. Sobel, H.L. Weiner, V.K. Kuchroo, and A.H. Sharpe. 2005. The ICOS molecule plays a crucial role in the development of mucosal tolerance. *J. Immunol.* 175: 7341–7347. <https://doi.org/10.4049/jimmunol.175.11.7341>
- Molofsky, A.B., J.C. Nussbaum, H.-E. Liang, S.J. Van Dyken, L.E. Cheng, A. Mohapatra, A. Chawla, and R.M. Locksley. 2013. Innate lymphoid type 2 cells sustain visceral adipose tissue eosinophils and alternatively activated macrophages. *J. Exp. Med.* 210:535–549. <https://doi.org/10.1084/jem.20121964>
- Molofsky, A.B., F. Van Gool, H.-E.E. Liang, S.J. Van Dyken, J.C. Nussbaum, J. Lee, J.A. Bluestone, and R.M. Locksley. 2015. Interleukin-33 and Interferon- $\gamma$  counter-regulate group 2 innate lymphoid cell activation during immune perturbation. *Immunity*. 43:161–174. <https://doi.org/10.1016/j.immuni.2015.05.019>
- Nagakubo, D., O. Yoshie, and T. Hirata. 2016. Upregulated CCL28 expression in the nasal mucosa in experimental allergic rhinitis: Implication for CD4(+) memory T cell recruitment. *Cell. Immunol.* 302:58–62. <https://doi.org/10.1016/j.cellimm.2016.02.001>
- Nishioka, T., J. Shimizu, R. Iida, S. Yamazaki, and S. Sakaguchi. 2006. CD4+CD25+Foxp3+ T cells and CD4+CD25-Foxp3+ T cells in aged mice. *J. Immunol.* 176:6586–6593. <https://doi.org/10.4049/jimmunol.176.11.6586>
- Noval Rivas, M., and T.A. Chatila. 2016. Regulatory T cells in allergic diseases. *J. Allergy Clin. Immunol.* 138:639–652. <https://doi.org/10.1016/j.jaci.2016.06.003>
- O'Brien, C.A., S.J. Batista, K.M. Still, and T.H. Harris. 2019. IL-10 and ICOS differentially regulate T cell responses in the brain during chronic *Toxoplasma gondii* infection. *J. Immunol.* 202:1755–1766. <https://doi.org/10.4049/jimmunol.1801229>
- Okamoto, N., K. Tezuka, M. Kato, R. Abe, and T. Tsuji. 2003. PI3-kinase and MAP-kinase signaling cascades in AILIM/ICOS- and CD28-costimulated T-cells have distinct functions between cell proliferation and IL-10 production. *Biochem. Biophys. Res. Commun.* 310:691–702. <https://doi.org/10.1016/j.bbrc.2003.09.065>
- Ono, M., H. Yaguchi, N. Ohkura, I. Kitabayashi, Y. Nagamura, T. Nomura, Y. Miyachi, T. Tsukada, and S. Sakaguchi. 2007. Foxp3 controls regulatory T-cell function by interacting with AML1/Runx1. *Nature*. 446:685–689. <https://doi.org/10.1038/nature05673>
- Panneton, V., J. Chang, M. Witalis, J. Li, and W.-K. Suh. 2019. Inducible T-cell co-stimulator: Signaling mechanisms in T follicular helper cells and beyond. *Immunol. Rev.* 291:91–103. <https://doi.org/10.1111/imr.12771>
- Pettersson, U.S., T.B. Waldén, P.-O. Carlsson, L. Jansson, and M. Phillipson. 2012. Female mice are protected against high-fat diet induced metabolic syndrome and increase the regulatory T cell population in adipose tissue. *PLoS One*. 7:e46057. <https://doi.org/10.1371/journal.pone.0046057>
- Rajbhandari, P., B.J. Thomas, A.-C. Feng, C. Hong, J. Wang, L. Vergnes, T. Sallam, B. Wang, J. Sandhu, M.M. Seldin, et al. 2018. IL-10 signaling remodels adipose chromatin architecture to limit thermogenesis and energy expenditure. *Cell*. 172:218–233.e17. <https://doi.org/10.1016/j.cell.2017.11.019>
- Redpath, S.A., N. van der Werf, A.M. Cervera, A.S. MacDonald, D. Gray, R.M. Maizels, and M.D. Taylor. 2013. ICOS controls Foxp3(+) regulatory T-cell expansion, maintenance and IL-10 production during helminth infection. *Eur. J. Immunol.* 43:705–715. <https://doi.org/10.1002/eji.201242794>
- Sather, B.D., P. Treuting, N. Perdue, M. Miazgowiec, J.D. Fontenot, A.Y. Rudensky, and D.J. Campbell. 2007. Altering the distribution of Foxp3(+) regulatory T cells results in tissue-specific inflammatory disease. *J. Exp. Med.* 204:1335–1347. <https://doi.org/10.1084/jem.20070081>

- Schmitz, J., A. Owyang, E. Oldham, Y. Song, E. Murphy, T.K. McClanahan, G. Zurawski, M. Moshrefi, J. Qin, X. Li, et al. 2005. IL-33, an interleukin-1-like cytokine that signals via the IL-1 receptor-related protein ST2 and induces T helper type 2-associated cytokines. *Immunity*. 23:479–490. <https://doi.org/10.1016/j.immuni.2005.09.015>
- Setoguchi, R., S. Hori, T. Takahashi, and S. Sakaguchi. 2005. Homeostatic maintenance of natural Foxp3(+) CD25(+) CD4(+) regulatory T cells by interleukin (IL)-2 and induction of autoimmune disease by IL-2 neutralization. *J. Exp. Med.* 201:723–735. <https://doi.org/10.1084/jem.20041982>
- Smigiel, K.S., S. Srivastava, J.M. Stolley, and D.J. Campbell. 2014a. Regulatory T-cell homeostasis: steady-state maintenance and modulation during inflammation. *Immunol. Rev.* 259:40–59. <https://doi.org/10.1111/imr.12170>
- Smigiel, K.S., E. Richards, S. Srivastava, K.R. Thomas, J.C. Dudda, K.D. Klonowski, and D.J. Campbell. 2014b. CCR7 provides localized access to IL-2 and defines homeostatically distinct regulatory T cell subsets. *J. Exp. Med.* 211:121–136. <https://doi.org/10.1084/jem.20131142>
- So, L., and D.A. Fruman. 2012. PI3K signalling in B- and T-lymphocytes: new developments and therapeutic advances. *Biochem. J.* 442:465–481. <https://doi.org/10.1042/BJ20112092>
- Stolley, J.M., and D.J. Campbell. 2016. A 33D1+ dendritic cell/autoreactive CD4+ T cell circuit maintains IL-2-dependent regulatory T cells in the spleen. *J. Immunol.* 197:2635–2645. <https://doi.org/10.4049/jimmunol.1600974>
- Tang, Q., K.J. Henriksen, E.K. Boden, A.J. Tooley, J. Ye, S.K. Subudhi, X.X. Zheng, T.B. Strom, and J.A. Bluestone. 2003. Cutting edge: CD28 controls peripheral homeostasis of CD4+CD25+ regulatory T cells. *J. Immunol.* 171:3348–3352. <https://doi.org/10.4049/jimmunol.171.7.3348>
- Vasanthakumar, A., K. Moro, A. Xin, Y. Liao, R. Gloury, S. Kawamoto, S. Fagarasan, L.A. Mielke, S. Afshar-Sterle, S.L. Masters, et al. 2015. The transcriptional regulators IRF4, BATF and IL-33 orchestrate development and maintenance of adipose tissue-resident regulatory T cells. *Nat. Immunol.* 16:276–285. <https://doi.org/10.1038/ni.3085>
- Vasanthakumar, A., D. Chisanga, J. Blume, R. Gloury, K. Britt, D.C. Henstridge, Y. Zhan, S.V. Torres, S. Liene, N. Collins, et al. 2020. Sex-specific adipose tissue imprinting of regulatory T cells. *Nature*. 579:581–585. <https://doi.org/10.1038/s41586-020-2040-3>
- Wan, Y.Y., and R.A. Flavell. 2005. Identifying Foxp3-expressing suppressor T cells with a bicistronic reporter. *Proc. Natl. Acad. Sci. USA*. 102:5126–5131. <https://doi.org/10.1073/pnas.0501701102>
- Wan, Z., X. Shao, X. Ji, L. Dong, J. Wei, Z. Xiong, W. Liu, and H. Qi. 2020. Transmembrane domain-mediated Lck association underlies bystander and costimulatory ICOS signaling. *Cell. Mol. Immunol.* 17:143–152. <https://doi.org/10.1038/s41423-018-0183-z>
- Wu, Y., M. Borde, V. Heissmeyer, M. Feuerer, A.D. Lapan, J.C. Stroud, D.L. Bates, L. Guo, A. Han, S.F. Ziegler, et al. 2006. FOXP3 controls regulatory T cell function through cooperation with NFAT. *Cell*. 126:375–387. <https://doi.org/10.1016/j.cell.2006.05.042>
- Wu, D., Z. Ren, M. Pae, W. Guo, X. Cui, A.H. Merrill, and S.N. Meydani. 2007. Aging up-regulates expression of inflammatory mediators in mouse adipose tissue. *J. Immunol.* 179:4829–4839. <https://doi.org/10.4049/jimmunol.179.7.4829>
- Wu, D., A.B. Molofsky, H.-E.E. Liang, R.R. Ricardo-Gonzalez, H.A. Jouihan, J.K. Bando, A. Chawla, and R.M. Locksley. 2011. Eosinophils sustain adipose alternatively activated macrophages associated with glucose homeostasis. *Science*. 332:243–247. <https://doi.org/10.1126/science.1201475>
- Wu, D., C.K. Wong, J.M. Han, P.C. Orban, Q. Huang, J. Gillies, M. Mojibian, W.T. Gibson, and M.K. Levings. 2020. T reg-specific insulin receptor deletion prevents diet-induced and age-associated metabolic syndrome. *J. Exp. Med.* 217:e20191542. <https://doi.org/10.1084/jem.20191542>
- Yamaguchi, T., J.B. Wing, and S. Sakaguchi. 2011. Two modes of immune suppression by Foxp3(+) regulatory T cells under inflammatory or non-inflammatory conditions. *Semin. Immunol.* 23:424–430. <https://doi.org/10.1016/j.smim.2011.10.002>

Supplemental material

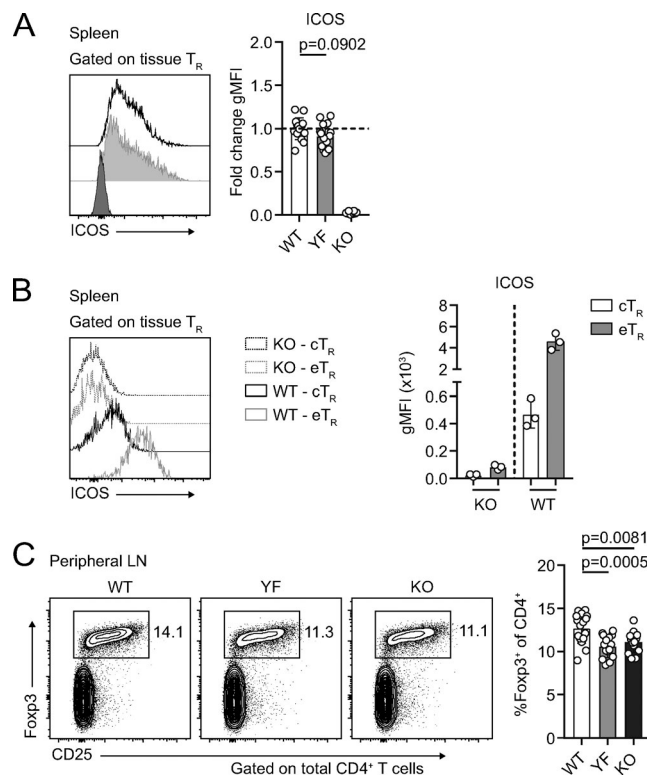


Figure S1. **Despite normal surface expression of ICOS, YF mice phenocopy KO with equivalent loss of lymphoid  $T_R$ s (goes with Fig. 1).** (A) ICOS expression on gated WT, YF, and KO splenic  $T_R$ s. Fold change of ICOS gMFI is compared with average expression in WT  $T_R$  for each individual experiment. Dashed line marks average value of WT control samples ( $n = 3$  per group from five independent experiments). (B) Representative ICOS expression on gated splenic KO and WT CD44<sup>lo</sup>CD62L<sup>hi</sup> c $T_R$  and CD44<sup>hi</sup>CD62L<sup>lo</sup> e $T_R$ s as measured by flow cytometry ( $n = 3$  per group from five independent experiments). (C)  $T_R$  frequencies of total  $CD4^+$  T cells in pLNs ( $n = 2-5$  per group from five independent experiments). Mice were age matched within individual experiments, and quantified data are pooled from experiments using male mice 8–16 wk of age. Statistical significance was determined using one-way ANOVA with Tukey’s post-test. All data are presented as mean values  $\pm$  SD.

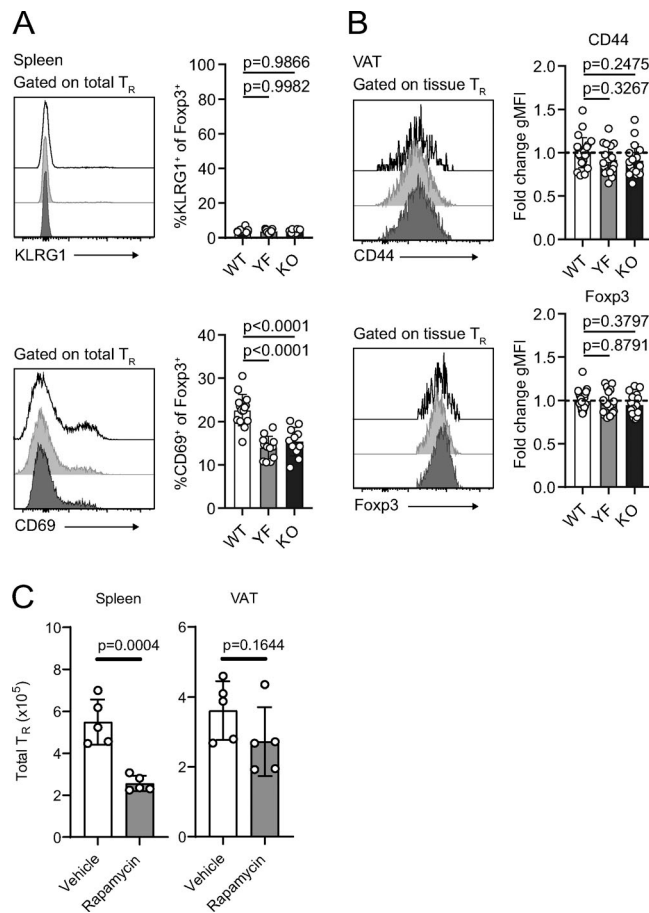


Figure S2. **Expression of activation markers on splenic and VAT-T<sub>R</sub>s (goes with Fig. 3).** **(A)** KLRG1 and CD69 expression in gated WT, YF, and KO splenic T<sub>R</sub>s ( $n = 3-6$  per group from three independent experiments). **(B)** CD44 and Foxp3 expression in tissue-localized VAT-T<sub>R</sub>s. gMFI was calculated as fold change compared with average expression in WT T<sub>R</sub>s for each individual experiment ( $n = 3-6$  per group from six independent experiments). **(C)** Mice were age matched within individual experiments, and pooled data are from experiments using 8-16-wk-old male mice. Statistical significance was determined using one-way ANOVA with Tukey's post-test. **(C)** Number of CD4<sup>+</sup>Foxp3<sup>+</sup> T<sub>R</sub>s in spleen (left) and VAT (right) in mice treated with rapamycin (1 mg/kg) or vehicle as indicated ( $n = 5$  mice per group from one experiment). Statistical significance was determined using two-tailed unpaired Student's *t* test. All data are presented as mean values  $\pm$  SD.

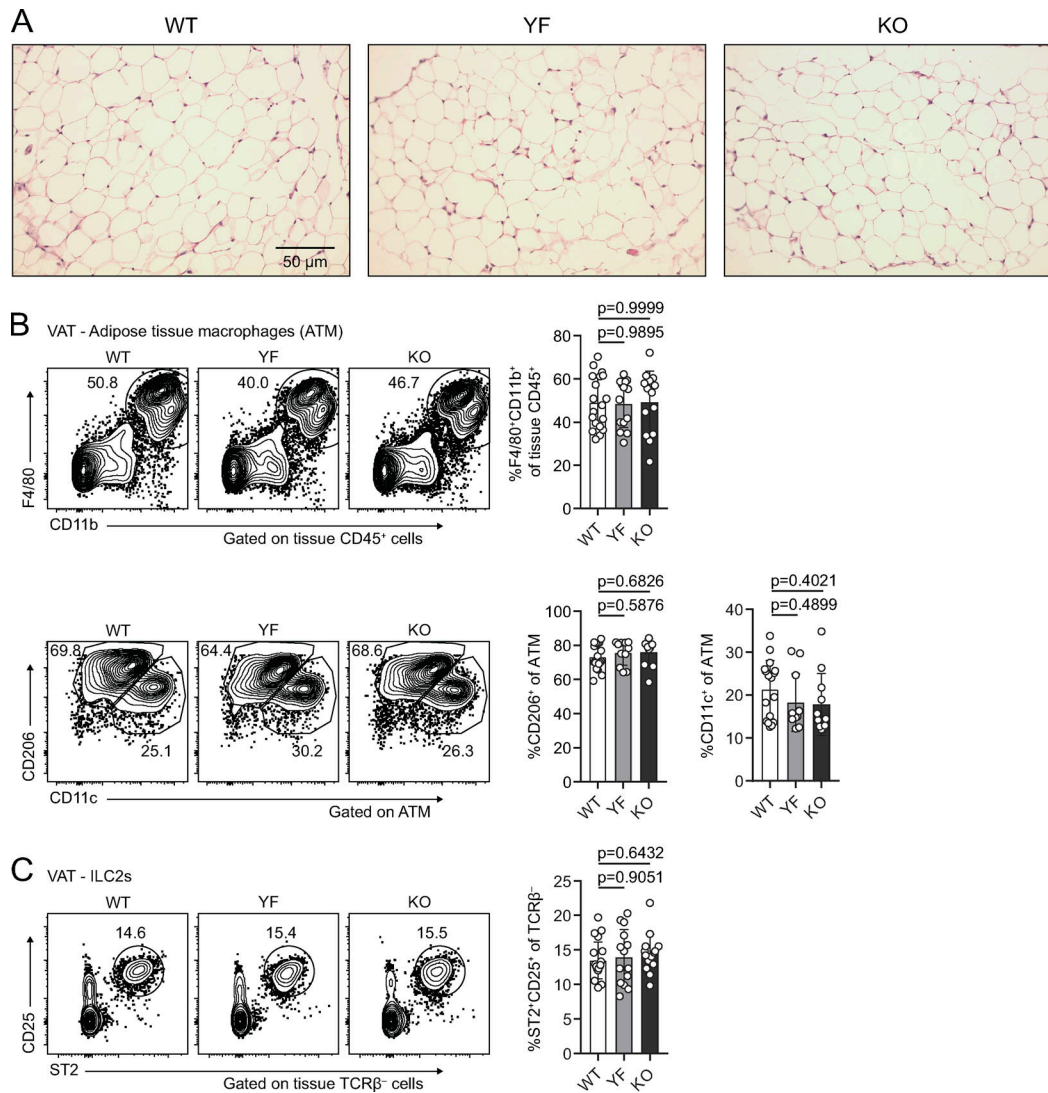


Figure S3. **Adipocyte, ATM, and ILC2 populations are unchanged in YF and KO VAT (goes with Fig. 4).** (A) H&E staining of VAT from 8-wk-old male mice. (B) Representative flow cytometry plots and quantification of tissue-localized ATM in WT, YF, and KO mice (top). Representative gating of ATM on CD11c and CD206 to identify M1-like and M2-like macrophages, respectively (bottom;  $n = 2-6$  per group from six independent experiments). (C) Frequency of tissue-localized ILC2s in VAT as measured by flow cytometry ( $n = 2-6$  per group from six independent experiments). Mice were age matched within individual experiments, and pooled data are from experiments using 8–16-wk-old male mice. Statistical significance was determined using one-way ANOVA with Tukey's post-test. All data are presented as mean values  $\pm$  SD.

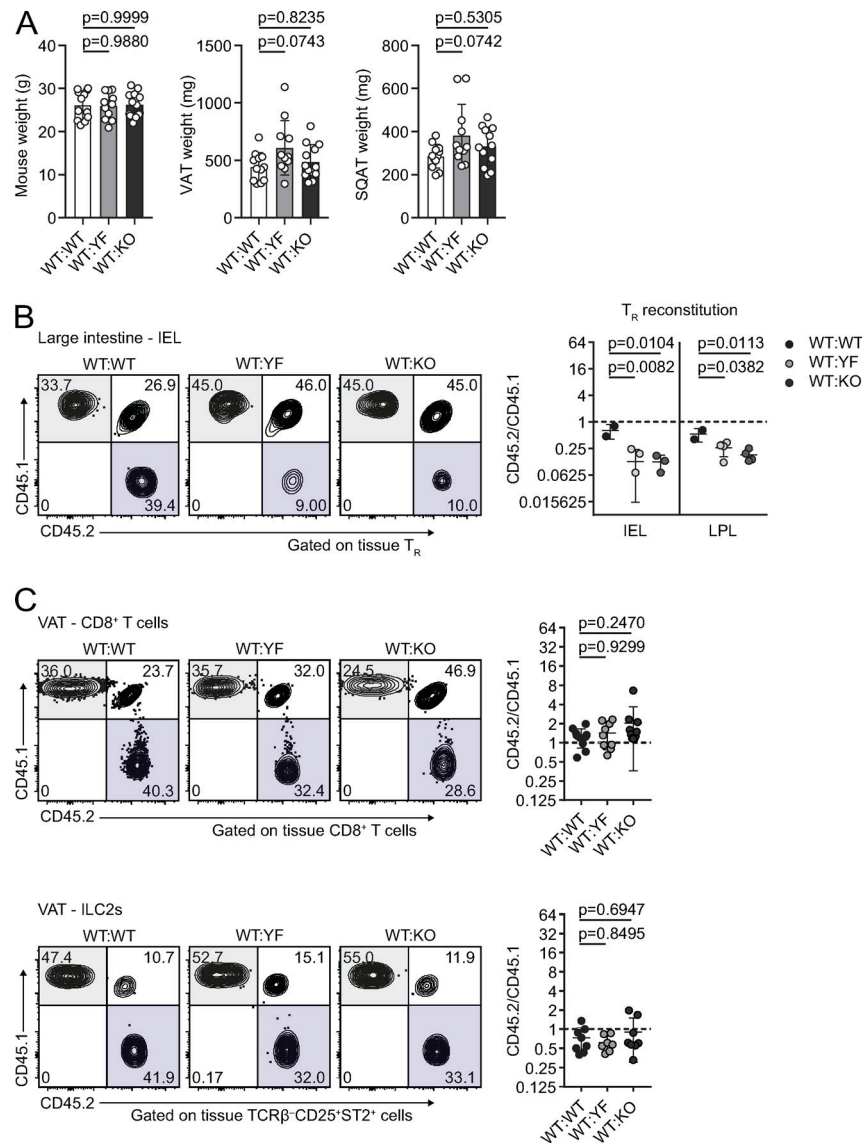


Figure S4. **Cell- and tissue-specific changes in reconstitution in ICOS mutant mixed bone marrow chimeras (goes with Fig. 6).** (A) Summary of total mouse (left), VAT (middle), and SQAT (right) weights in mixed bone marrow chimeras. (B) Representative gating of CD45.1 versus CD45.2 expression on tissue-restricted T<sub>R</sub>s in IELs from the large intestine. Graphs summarize reconstitution of donor T<sub>R</sub>s of IELs and lamina propria lymphocytes (LPLs) in the large intestine. (C) Representative gating of CD45.1 versus CD45.2 expression in chimeric mice on total CD8<sup>+</sup> T cells (top) and ILC2s (bottom) in VAT. Graphs summarize reconstitution of donor CD8<sup>+</sup> T cells (top) and ILC2s (bottom) in VAT. Dashed lines in all graphs indicate a CD45.2/CD45.1 ratio of 1. Data are pooled from three independent mixed bone marrow chimera experiments with *n* = 3–5 male chimeric mice per group. Statistical significance was determined using one-way ANOVA with Tukey's post-test for each individual tissue. All data are presented as mean values ± SD.

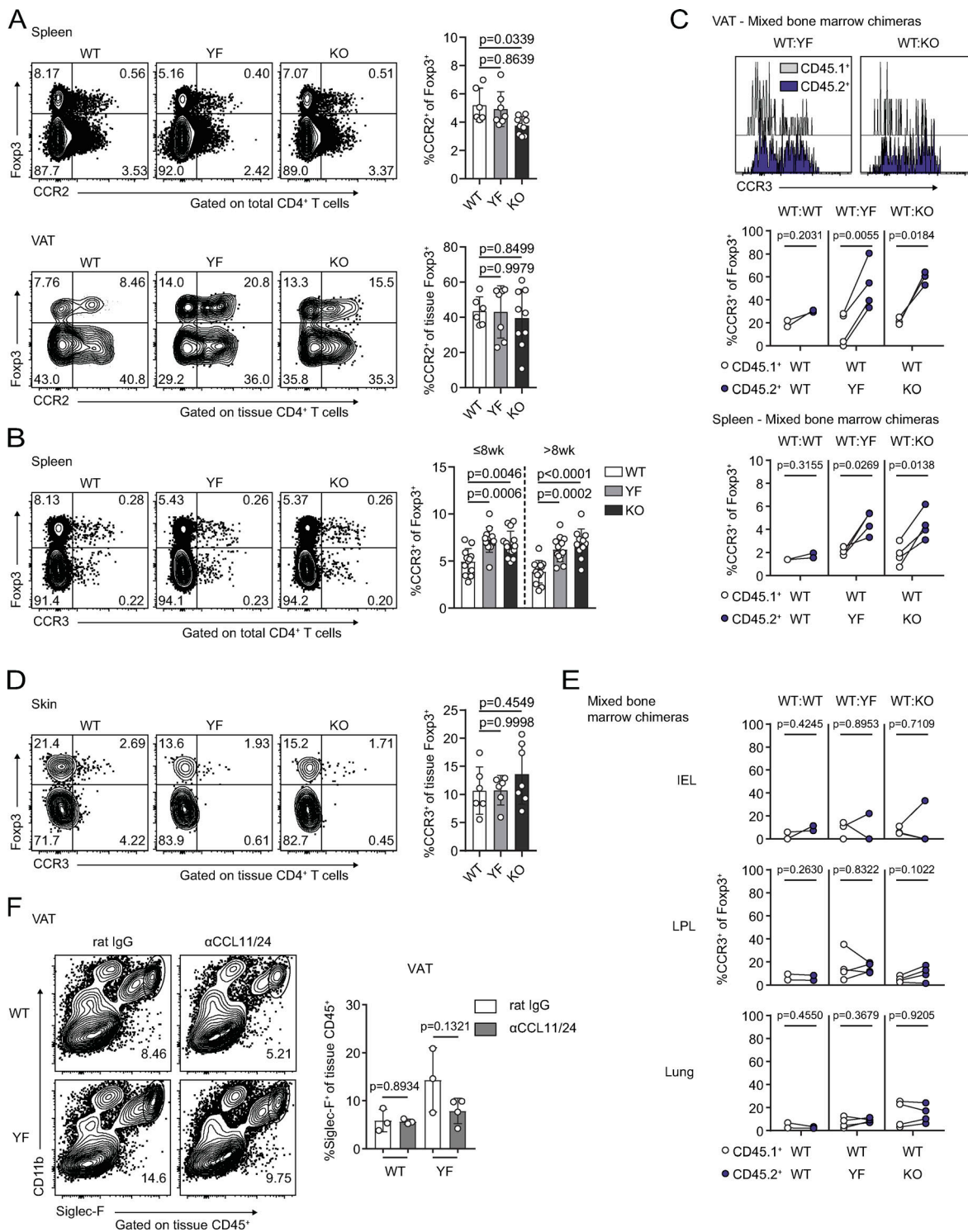


Figure S5. **Increased accumulation of CCR3<sup>+</sup> T<sub>R</sub>s in the absence of ICOS signaling is specific to VAT (goes with Fig. 8).** (A) CCR2 expression by splenic (top) and VAT-T<sub>R</sub>s (bottom) as measured by flow cytometry ( $n = 3-5$  per group from two independent experiments). (B) Expression of CCR3 in splenic T<sub>R</sub>s in mice  $\leq 8$  wk and  $> 8$  wk of age ( $n = 3-5$  per group from seven independent experiments). (C) Expression of CCR3 by gated CD45.1<sup>+</sup> and CD45.2<sup>+</sup> donor VAT-T<sub>R</sub>s in chimeric mice. Graphs summarize CCR3 expression by donor T<sub>R</sub>s in VAT and spleen. Line connects point representing CD45.1<sup>+</sup> and CD45.2<sup>+</sup> cells within the same chimeric mouse ( $n = 2-4$  per group from two independent experiments). (D) CCR3 expression by tissue-localized skin T<sub>R</sub>s as measured by flow cytometry ( $n = 2-4$  per group from two independent experiments). (E) CCR3 expression by CD45.1<sup>+</sup> and CD45.2<sup>+</sup> donor T<sub>R</sub>s within the same chimeric mouse in indicated tissues. Line connects CD45.1<sup>+</sup> and CD45.2<sup>+</sup> cells within the same chimeric mouse ( $n = 2-4$  per group from two independent experiments). (F) Frequency of tissue-restricted VAT eosinophils with and without in vivo CCL11/24 blockade as measured by flow cytometry ( $n = 3$  or 4 mice per group). Mice were age matched within individual experiments, and pooled data are from experiments using 8-16-wk-old male mice. Statistical significance was determined using one-way ANOVA with Tukey's post-test (A, B, and D); two-tailed, paired Student's *t* test for expression in donor cells within the same chimeric mouse (C and E); and two-tailed Student's *t* test (F). All data are presented as mean values  $\pm$  SD. IEL, lamina propria lymphocyte.